CARDIFF UNIVERSITY
PRIFYSGOL CAERDYDD

ORCA – Online Research @ Cardiff

This is an Open Access document downloaded from ORCA, Cardiff University's institutional repository:https://orca.cardiff.ac.uk/id/eprint/162228/

This is the author's version of a work that was submitted to / accepted for publication.

Citation for final published version:

Bekheit, Mohamed S., Panda, Siva S., Kariuki, Benson M. , Mahmoud, Sara H., Mostafa, Ahmed and Girgis, Adel S. 2023. Spiroindole-containing compounds bearing phosphonate group of potential Mpro-SARS-CoV-2 inhibitory properties. European Journal of Medicinal Chemistry 258 , 115563. 10.1016/j.ejmech.2023.115563

Publishers page: http://dx.doi.org/10.1016/j.ejmech.2023.115563

Please note:
Changes made as a result of publishing processes such as copy-editing, formatting and page numbers may not be reflected in this version. For the definitive version of this publication, please refer to the published source. You are advised to consult the publisher's version if you wish to cite this paper.

This version is being made available in accordance with publisher policies. See http://orca.cf.ac.uk/policies.html for usage policies. Copyright and moral rights for publications made available in ORCA are retained by the copyright holders.

Research paper

Spiroindole-containing compounds bearing phosphonate group of potential M^{pro}-SARS-CoV-2 inhibitory properties

Mohamed S. Bekheit [a], Siva S. Panda [b], Benson M. Kariuki [c], Sara H. Mahmoud [d], Ahmed Mostafa [d], Adel S. Girgis [a,*]

[a] Department of Pesticide Chemistry, National Research Centre, Dokki, Giza, 12622, Egypt
[b] Department of Chemistry and Physics, Augusta University, Augusta, GA, 30912, USA
[c] School of Chemistry, Cardiff University, Main Building, Park Place, Cardiff, CF10 3AT, UK
[d] Center of Scientific Excellence for Influenza Viruses, National Research Centre, Giza, 12622, Egypt

ARTICLEINFO

Keywords:
Spiroindole
Phosphonate
Azomethine ylide
SARS-CoV-2
COVID-19

ABSTRACT

Microwave-assisted reaction of 3,5-bis((*E*)-ylidene)-1-phosphonate-4-piperidones **3a–g** with azomethine ylide (produced through interaction of isatins **4** and sarcosine **5**) cycloaddition afforded the corresponding (dispiro [indoline-3,2′-pyrrolidine-3′,3′′-piperidin]-1′′-yl)phosphonates **6a–l** in excellent yields (80–95%). Structure of the synthesized agents was evidenced by single crystal X-ray studies of **6d**, **6i** and **6l**. Some of the synthesized agents revealed promising anti-SARS-CoV-2 properties in the viral infected Vero-E6 cell technique with noticeable selectivity indices. Compounds **6g** and **6b** are the most promising agents synthesized (R = 4-BrC_6H_4, Ph; R′ = H, Cl, respectively) with considerable selectivity index values. M^{pro}-SARS-CoV-2 inhibitory properties supported the anti-SARS-CoV-2 observations of the potent analogs synthesized. Molecular docking studies (PDB ID: 7C8U) are consistent with the M^{pro} inhibitory properties. The presumed mode of action was supported by both experimentally investigated M^{pro}-SARS-CoV-2 inhibitory properties and explained by docking observations.

1. Introduction

The calamitous global pandemic due to the COVID-19 (coronavirus disease 2019) is one of the most widespread in recorded history. The SARS-CoV-2 (severe acute respiratory syndrome coronavirus-2) put the entire world under social and economic stress due to its high infectivity. An aggravating factor was the limited access to urgent medical treatment for a large proportion of the world population. Initial discovery of the disease was associated with local fish and wild animals market in Wuhan, China, towards the end of 2019 when it started spreading rapidly worldwide effectively impacting all countries and nations. Lack of principal knowledge concerning the cell biology of the new virus with high prevalence and fatality rate compelled the entire scientific society to explore for promising pathways to save human life and avoid socio-economic disaster [1].

SARS-CoV-2 is an RNA zoonotic virus belonging to the *Coronaviridae* family, order: *Nidovirales*, genus: *Betacoronavirus*. It is commonly found in bats but, for unclear reasons, became infectious with the ability to transfer from human to human thereby spreading worldwide resulting in a global pandemic [2,3]. It is a positive-sense single-stranded RNA virus (ssRNA(+)) with genetic material capable of performing the function of messenger RNA (mRNA) [4–6].

The number of infected patients and mortality increased dramatically after the first alarm was raised (pandemic status was declared by the World health organization (WHO) in March 2019) [7]. About 761.4 million infected patients and 6.887 million deaths were confirmed by WHO [8]. Symptoms due to SARS-CoV-2 infection are similar to many other diseases (for example flu) and include; cough, headache, fever, diarrhea, breathing difficulty, and loss of taste and/or smell. For severe cases, supplemental oxygen and intensive care hospitalization are needed due to respiratory problems that can seriously impact human organ function and possibly lead to death. Several waves of SARS-CoV-2 mutants were observed, namely: Alpha (B.1.1.7), Beta (B.1.351), Gamma (P.1), Delta (B.1.617.2), Epsilon (B.1.427 and B.1.429), Eta (B.1.525), Iota (B.1.526), Kappa (B.1.617.1), Mu (B.1.621, B.1.621.1) and Zeta (P.2). The Omicron (B.1.1.529) variant was first identified in Botswana in Nov. 2021 and rapidly spread to all countries worldwide [9–12]. The Omicron variant is highly efficiently transmitted between

* Corresponding author.
E-mail addresses: girgisas10@yahoo.com, as.girgis@nrc.sci.eg (A.S. Girgis).

humans. Due to the continuous virus mutation and limitation of effective therapeutics, it is estimated that the epidemic disease is away from its end [13].

Some proteins have been mentioned as having a critical role in SARS-CoV-2 infection making them potential targets for optimizing therapeutic agents (Fig. 1) [14]. Coronavirus main protease (M^{pro}, also called $3CL^{pro}$) plays an essential role in viral maturation, replication and transcription. Thus, the inhibition of M^{pro} is an attractive target for therapeutics against COVID-19 [15,16]. By the end of 2021, FDA (Food and Drug Administration) approved (under the emergency use authorization) Paxlovid as anti-SARS-CoV-2 therapeutic for mild and moderate COVID-19 patients. It is a combination of two effective agents, Nirmatrelvir (3CL protease inhibitor) and Ritonavir (protease inhibitor originally developed for HIV/AIDS). Paxlovid can reduce the risk of death or the hospitalization period if administrated within a few days of symptoms due to infection appearing [17−19]. PF-00835231 is an M^{pro} inhibitor (Ki = 0.27 nM) with potential inhibitory properties against SARS-CoV-2 [EC_{50} (Vero-E6 cell)= up to 0.23 μM] reported by Pfizer as a repurposing therapeutic (Fig. 2) [20]. 2-Substituted indolealkylamines were mentioned as potential anti-SARS-CoV-2 candidates with viral main protease (M^{pro}) inhibitory properties [21]. Many indole-containing compounds have also been mentioned by the in-silico studies as M^{pro} inhibitory properties but lack of experimental bio-evidence has hindered their applicability [15,22−25].

The scientific community pulled all stops to investigate and develop effective diagnostic and therapeutical agents in addition to vaccines capable of preventing infection [26]. Vaccination was considered as an integral part for controlling the long-term COVID-19 pandemic as the protective neutralizing antibodies produced in the human body that can either completely protect from infection or control the severe symptoms of the infectious virus. A number of vaccines with substantial efficacy against different variants of SARS-CoV-2 were developed and administered [27]. The most well-known are BNT162b2 by Pfizer/BioNTech, mRNA-1273 by Moderna, and AZD1222 by University of Oxford & AstraZeneca [28]. Large scale vaccination was pursued for controlling the infection as herd immunity was risky due to no certain evidence being available for acquired immunity in recovered COVID-19 patients [29]. Although convalescent plasma was considered as a therapeutic tool for severely infected patients, the feasibility of this approach was questionable [30].

Drug repurposing has been the main technique for identifying potential therapeutics against COVID-19. Investigating new drugs usually needs lots of research investigations requiring effort, time and money. However, redirecting already known drugs towards a new disease is an attractive shortcut towards the desired target. Many repurposed therapeutics have been identified with potential potency for mild and moderate infections [31]. However, none up to our knowledge has efficacy for severe conditions. Arbidol (an indolyl scaffold) is a broad spectrum antiviral agent (anti-influenza, hepatitis "HBV, HCV", Ebola, Lassa, and chikungunya) with hemagglutinin esterase inhibitory properties. It was successfully repurposed against COVID-19 [32−38]. Obatoclax which

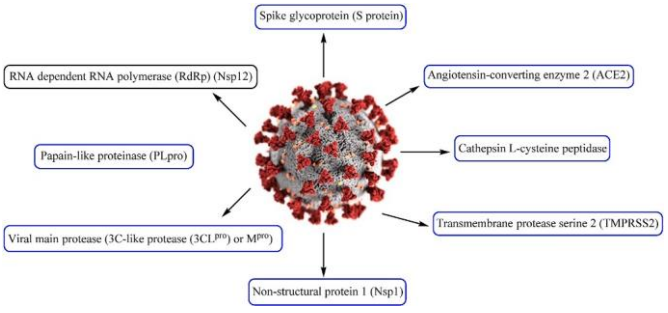

Fig. 1. Some of the proteins involved in the SARS-CoV-2 infection, that make them potential targets for developing therapeutical agents.

was subjected to phase II clinical trial as an anticancer agent (leukemia, lymphoma, and lung) revealed potent anti-SARSCoV-2 properties in addition to the inhibitory properties against S protein-mediated virus entry suggesting its potenial applicibility against COVID-19 [39]. Melatonin which is a natural product found in plants and animals with antioxidant and anti-inflammatory properties was mentioned as a promising agent useful for preventing and treating COVID-19 with safety profile. Reports supported that treatment of COVID-19 patients with melatonin alone or in combination with another therapeutic drug either shortened the hospitalization period or reduced the severity of the viral infection (Fig. 2) [40−47].

The current study is directed towards construction of new spiroindole-containing compounds bearing a phosphonate moiety. Interest of this scaffold is attributed to the previously described anti-COVID-19 properties of indole-containing heterocycles especially those considered repurposed drug (Arbidol) and the potent clinically supported ones (PF-00835231, Obatoclax and Melatonin). The potent anti-SARS-CoV-2 properties of indole and spiroindole-containing analogs also encouraged the current study [48,49]. Interest in insertion of the phosphoryl group into the heterocyclic system is the ability of the group to improve the physicochemical properties as the electron-rich phosphoryl residue that may increase the bioavailability of the targeted agents [50]. Previous reports describing the antiviral properties of phosphonate-containing compounds also support the rationality of the current design study [51,52]. Many therapeutics incorporating the phosphonate group are well known and include Etidronate [53], Pamidronate [54], Alendronate [55], Zoledronic acid [56], Ibandronic acid [57] (FDA approved in 1977, 1991, 1995, 2001, 2003 for osteoporosis) and Amifostine (FDA approved in 1995 to reduce kidney toxicity "nephrotoxic" effect upon repeated treatment of ovarian cancer with cisplatin) [58,59] (Fig. 3).

2. Results and discussion

2.1. Chemical synthesis

The *N*-diethyl phosphonate-4-piperidones **3a−g** were synthesized in good to excellent yields (71–87%) through dehydrohalogenation reaction of diethylchlorophosphate **2** with 3,5-bis(ylidene)-4-piperidones **1a−g** in DMF (*N*,*N*-dimethylformamide) in presence of a sufficient amount of TEA (triethylamine) at 0 °C. The single signal integrated to two protons at δ_H 7.67–7.89 evidenced the *E*-configuration [60−63]. Azomethine cycloaddition (obtained through condensation of sarcosine **5** with isatins **4**) with the appropriate *N*-diethyl phosphonate-4-piperidones **3a−g** in ethanolic solution under micro- wave condition (60 Watt, 60 °C) gave the targeted spiroindoles **6a−l** in excellent yields (80–95%) as the only isolable products (Scheme 1). The spectral data (IR, ^{1}H, ^{13}C NMR, ^{1}H, ^{1}H-Cosy, and HSQC) evidenced the chemical structure (Supplementary information file Fig. S1−S59).

2.2. X-ray studies

The molecule of **6d** is shown in Fig. 4. In the diethyl phosphonate group (P1, O3 – O5, C30 – C33); one ethoxy group is disordered with two components. The P–O–C–C bonds are in trans conformation (except for one disorder component which is gauche). The pyrrolidine ring (C1, C10 – C12, N2) is in envelope conformation with the nitrogen located 0.574 (4) Å from the least squares plane through the other atoms. The pyrrolidine ring is linked to three other ring systems which are oriented perpendicular to its plane, namely: fluorophenyl (C13–C18, F1), chloroindol-2-one (C1 – C8, O1, N1, Cl1) and piperidone (C12, C19 – C22, O2, N3) rings. The piperidone ring is essentially planar except for atom N3 which deviates by 0.580(2) Å from the plane through the rest of the atoms. The fluorophenylmethylene group (C23–C29, F2) is twisted by about 40° from the plane of the piperidone ring.

The molecule of **6i** is shown in Fig. 5. In the diethyl phosphonate

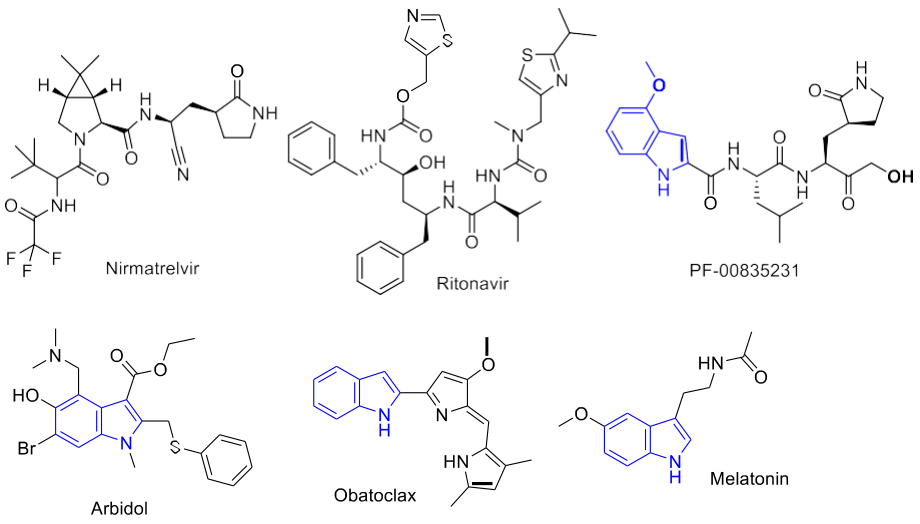

Fig. 2. Repurposed drugs against COVID-19.

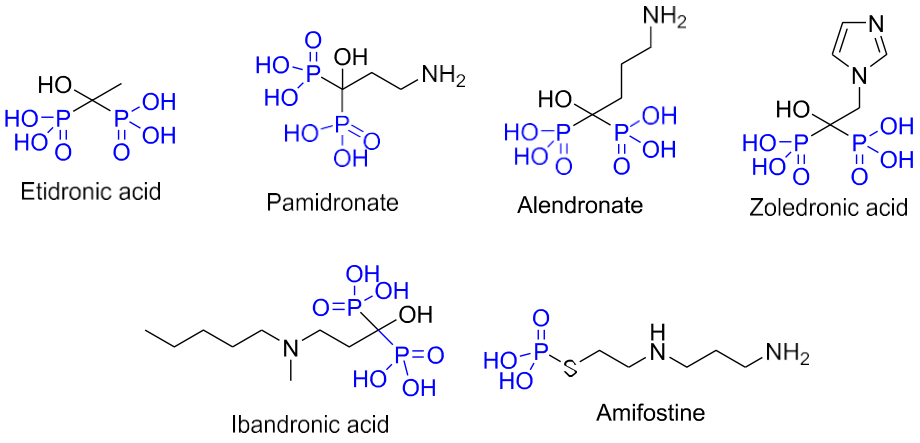

Fig. 3. Drugs with phosphonate group.

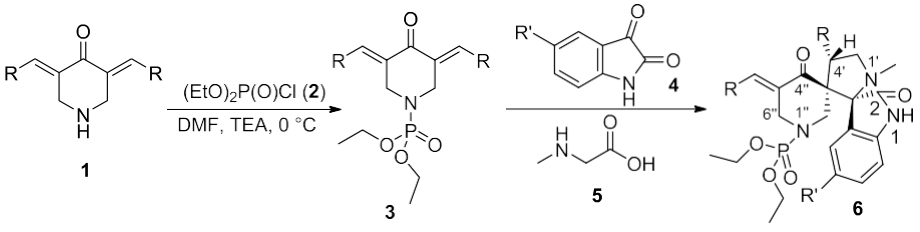

1a, **3a**; R = Ph
1b, **3b**; R = 4-FC_6H_4
1c, **3c**; R = 4-ClC_6H_4
1d, **3d**; R = 4-BrC_6H_4
1e, **3e**; R = 4-$H_3COC_6H_4$
1f, **3f**; R = 4-$H_3CC_6H_4$
1g, **3g**; R = 2-thienyl

4a, R' = H
4b, R' = Cl

6a; R = Ph, R' = H (92 %)
6b; R = Ph, R' = Cl (94 %)
6c; R = 4-FC_6H_4, R' = H (95 %)
6d; R = 4-FC_6H_4, R' = Cl (92 %)
6e; R = 4-ClC_6H_4, R' = H (91 %)
6f; R = 4-ClC_6H_4, R' = Cl (89 %)
6g; R = 4-BrC_6H_4, R' = H (85 %)
6h; R = 4-$H_3COC_6H_4$, R' = H (88 %)
6i; R = 4-$H_3CC_6H_4$, R' = H (96 %)
6j; R = 4-$H_3CC_6H_4$, R' = Cl (93 %)
6k; R = 2-thienyl, R' = H (84 %)
6l; R = 2-thienyl, R' = Cl (80 %)

Scheme 1. Synthetic route toward spiroindoles **6a–l**.

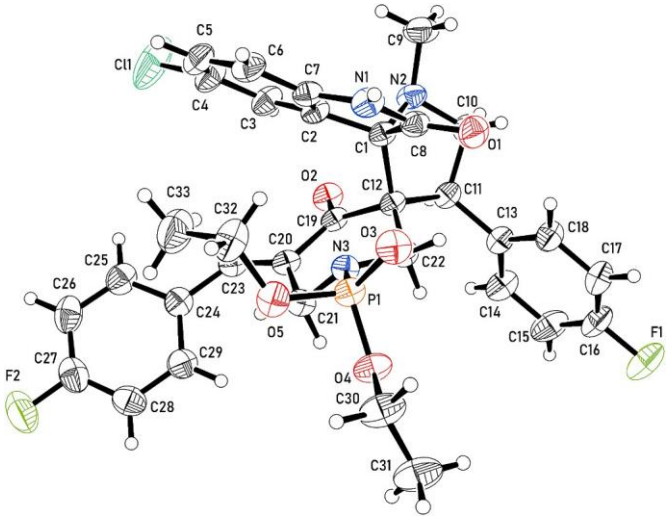

Fig. 4. An ortep representation of the asymmetric unit of the crystal structure of **6d** showing 50% probability atomic displacement ellipsoids for one disorder component.

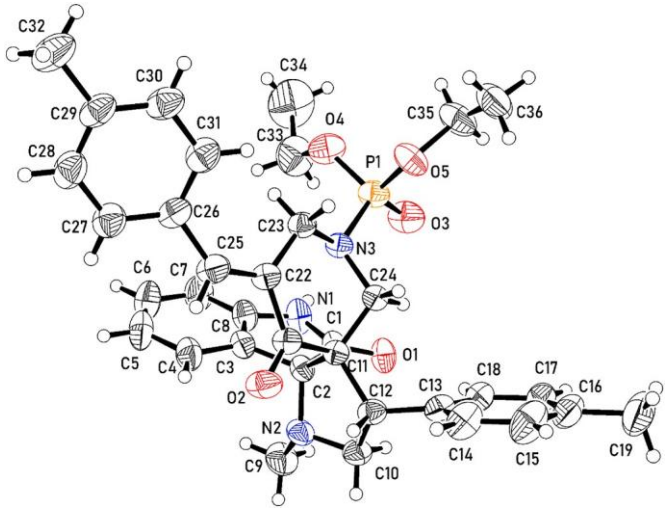

Fig. 5. An ortep representation of the asymmetric unit of the crystal structure of **6i** showing 50% probability atomic displacement ellipsoids for one disorder component.

group (P1, O3 – O5, C33 – C36), one P–O–C–C bond is in trans conformation and the second is gauche. The pyrrolidine ring (C2, C10 – C12, N2) is in envelope conformation with the nitrogen located 0.594 (3) Å from the least squares plane through the other atoms. The pyrrolidine ring is linked to three other ring systems which are oriented perpendicular to its plane, namely: methylphenyl (C13–C19), indol-2-one (C1 – C8, O1, N1) and piperidone (C11, C21 – C24, O2, N3) rings. The piperidone ring is essentially planar except for atom N3 which deviates by 0.462(2) Å from the plane through the rest of the atoms. The tolylmethylene group (C25–C32) is disordered with two components and is twisted by about 35° from the plane of the piperidone ring.

There are two unique molecules in the crystal of **6l** (Fig. 6). In both molecules, the thiophene ([C13 – C16, S1] for the first molecule and [C42 – C45, S3] for the second molecule), (thienyl)methylene ([C21 – C25, S2] for the first molecule and [C50 – C54, S4] for the second molecule), and the diethyl phosphonate ([P1, O3 – O5, C26 – C29] for the first molecule and [P2, O8 – O10, C55 – C58] for the second molecule) are disordered with two components. The P–O–C–C bonds are in trans conformation for the major components whereas one torsion of

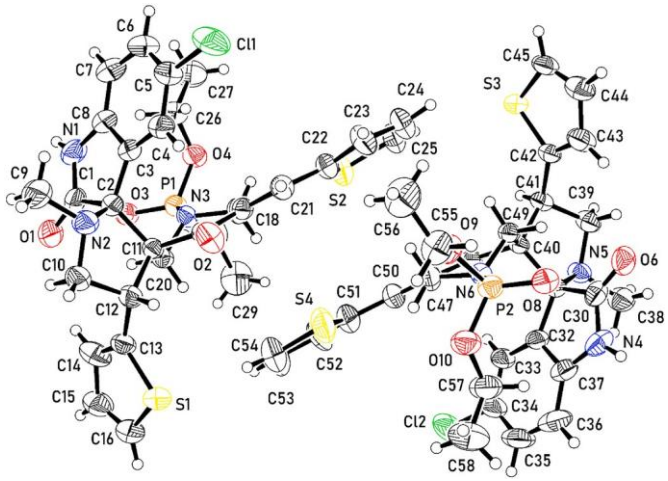

Fig. 6. An ortep representation of the asymmetric unit of the crystal structure of **6l** showing 50% probability atomic displacement ellipsoids for one disorder component.

each minor component of the molecule is gauche. The pyrrolidine rings ([C2, C10 – C12, N2] for the first molecule and [C31, C39 – C40, N5] for the second molecule) are in envelope conformation with the nitrogen atoms N2 and N5 being located 0.595 (4) Å and 0.596 (5) Å from the least squares plane through the other atoms of the respective rings. Each pyrrolidine ring is linked to three ring systems which are oriented perpendicular to its plane. These are thiophene, chloroindol-2-one ([C1 – C8, O1, N1, Cl1] for the first molecule and [C30 – C37, O6, N4, Cl2] for the second molecule) and piperidone ([C11, C17 – C20, O2, N3] for the first molecule and [C40, C46 – C49, O7, N6] for the second molecule) rings. The piperidone rings are essentially planar other than for atoms N3 and N6 which are located 0.503(3) Å and 0.541(3) Å from the planes through the rest of the atoms of their respective rings. The (thienyl) methylene group is nearly co-planar with the piperidone ring which is linked to.

The molecules of **6d**, **6i** and **6l** have a common core comprising pyrrolidine, indol-2-one and piperidone rings. This unit is relatively rigid with the same geometry in all three compounds. Any variation in the biological properties of these molecules, therefore can be reasonably attributed to the conformational flexibility of the pendant groups as well as their derivatization.

2.3. Anti-SARS-CoV-2 properties

The standard viral infected Vero-E6 cell technique was used to assess the anti-SARS-CoV-2 properties of the synthesized spiroindoles **6a–l** [64–66]. The results (Table 1, Fig. 7), indicate that some of the synthesized spiroindoles are more potent SARS-CoV-2 inhibitor than the standard references used (Favipiravir, Hydroxychloroquine and Chloroquine) with promising selectivity indices (SI). Of the synthesized agents, compound **6g** (R = 4-BrC_6H_4, R′ = H) is the most promising, with IC_{50} = 8.88 μM, CC_{50} = 20.33 μM, and SI = 2.29. Compound **6b** (R = Ph, R′ = Cl) also has comparable anti-SARS-CoV-2 properties (IC_{50} = 10.39 μM, CC_{50} = 22.0 μM, SI = 2.12) but with lower efficacy than **6g**. Although compound **6i** (R = 4-$H_3CC_6H_4$, R′ = H) exhibits a higher SI value relative to the other synthesized analogs (IC_{50} = 35.21 μM, CC_{50} = 87.01 μM, SI = 2.47), it has lower efficacy than **6g** and **6b**. Compound **6f** (R = 4-ClC_6H_4, R′ = Cl) displays higher anti-SARS-CoV-2 activity but with a lower SI value (IC_{50} 7.26 μM, CC_{50} 10.0 μM, SI 1.38) than those of **6g**, **6b** and **6i**. Similar observations are also made for compound **6d** (R = 4-FC_6H_4, R′ = Cl) and **6j** (R = 4-$H_3CC_6H_4$, R′ = Cl), The values for **6d**, **6j** are IC_{50} 13.53, 21.66 μM; CC_{50} 18.83, 40.10 μM; and SI = 1.39, 1.85 respectively.

SAR (structure-activity relationship) deduced from anti-SARS-CoV-2

Table 1
Anti-SARS-CoV-2 properties of the synthesized spiroindoles **6a–l** and standard references.

Compd.	IC_{50} (μM)	CC_{50} (μM)	Selectivity index (SI)
6a	88.61	73.07	0.82
6b	10.39	22.0	2.12
6c	85.84	126.0	1.47
6d	13.53	18.83	1.39
6e	340	9.834	0.03
6f	7.26	10.0	1.38
6g	8.88	20.33	2.29
6h	46.74	38.33	0.82
6i	35.21	87.01	2.47
6j	21.66	40.10	1.85
6k	106.1	49.92	0.47
6l	578.4	23.71	0.04
Favipiravir [65]	1382	5262	3.8
Hydroxychloroquine [61]	36.92	356.4	9.7
Chloroquine [61]	24.98	377.7	15.1

$SI = CC_{50}/IC_{50}$

activity indicate that the chloroindolyl-containing compounds have higher efficacy than the unsubstituted analogs (compound **6l** which contains thienyl heterocycle is an exception). This rule seems to apply to the synthesized compounds derived from (un)substitutd benzylidene-4-piperidones in general as supported by comparison of pairs **6a**/**6b** (IC_{50} = 88.61, 10.39 μM, respectively), **6c**/**6d** (IC_{50} = 85.84, 13.53 μM, respectively), **6e**/**6f** (IC_{50} = 340, 7.26 μM, respectively) and **6i**/**6j** (IC_{50} =35.21, 21.66 μM, respectively). These observations support the role of indolyl heterocyclic substitution in the anti-SARS-CoV-2 properties.

2.4. M^{pro}-SARS-CoV-2 properties

M^{pro} is one of the essential proteins for replication and gene expression of the SARS-CoV-2 virus. Inhibition of M^{pro} is considered one of the most potential pathways for treating infected COVID-19 patients [67]. The M^{pro} inhibitory properties of the most effective agents synthesized **6g**, **6b** and **6d** were determined by an appropriate Kit assay [68]. From the results (Table 2), compound **6b** has the most potent against M^{pro}-SARS-CoV-2 and is comparable to Tipranavir (IC_{50} = 9.605, 7.38 μM, respectively). Tipranavir (Fig. 8) is a non-peptidic protease inhibitor useable for therapy and prevention of HIV (human immunodeficiency virus) [69–71]. Spiroindole **6g** also shows promising M^{pro}-SARS-CoV-2 inhibitory properties (IC_{50} = 15.59 μM). Considerable

Table 2
IC_{50} values of M^{pro}-SARS-CoV-2 for the synthesized agents (**6b**, **6d** and **6g**) and standard reference Tipranavir.

Entry	Compd.	IC_{50} (μM ± SE)
1	**6b**	9.605 ± 0.66
2	**6d**	42.82 ± 2.53
3	**6g**	15.59 ± 1.02
4	**Tipranavir**	7.38 ± 0.42

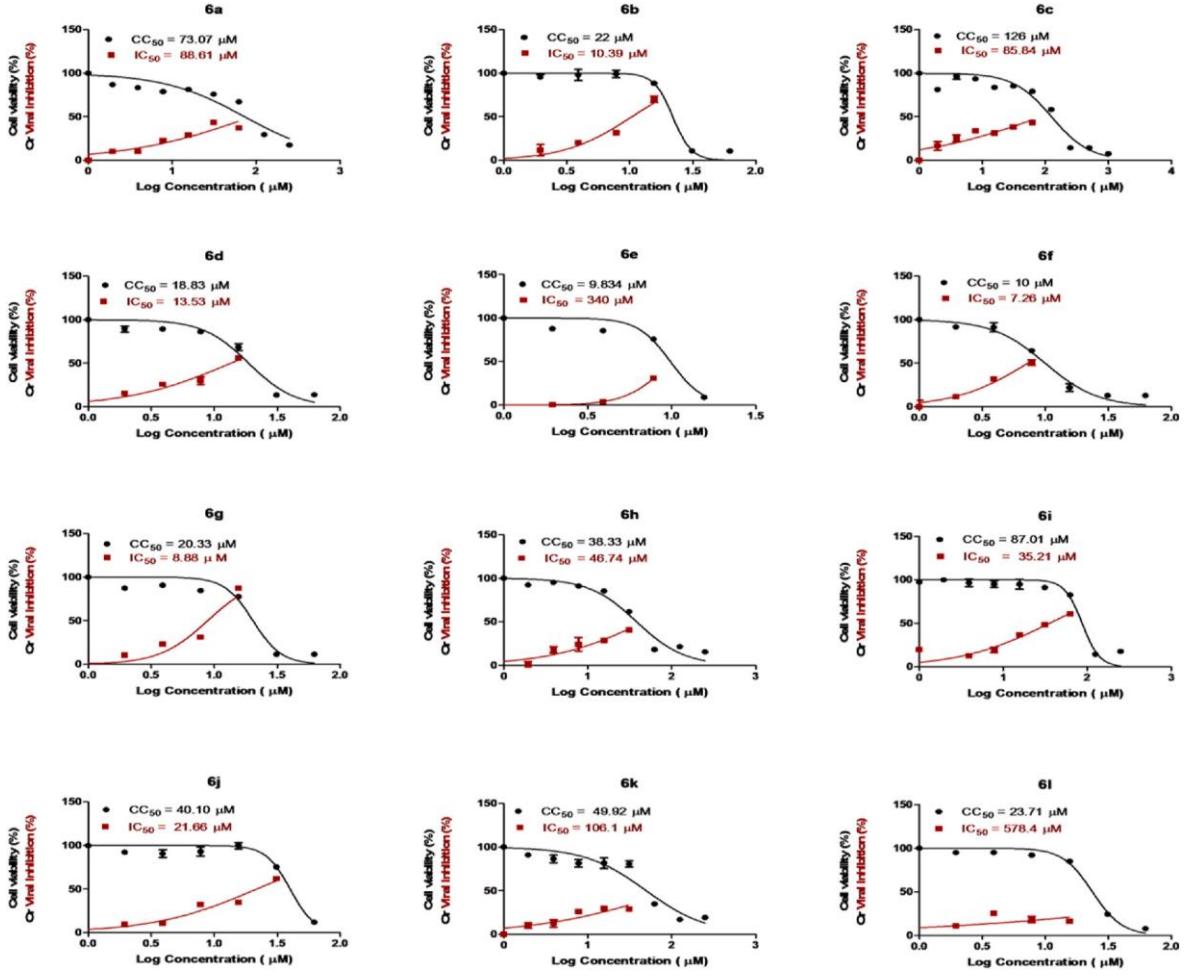

Fig. 7. Dose-response curves for the spiroindole **6a–l** against SARS-CoV-2.

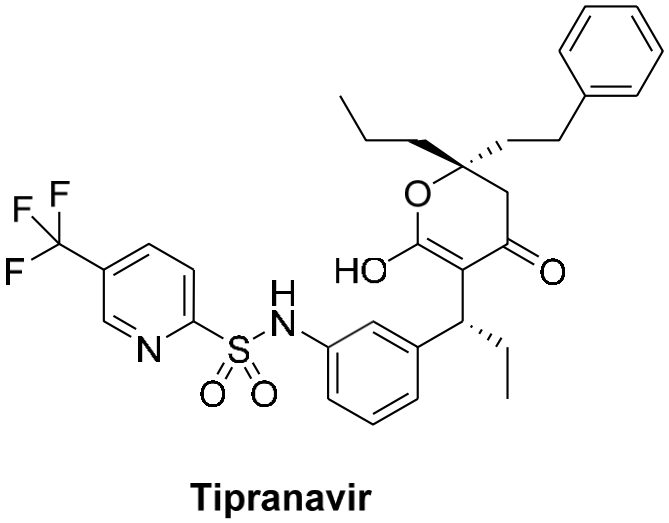

Tipranavir

Fig. 8. Tipranavir, protease inhibitor useable for therapy and prevention of HIV.

protease inhibitory properties are also shown by spiroindole **6d** (IC_{50} = 42.82 μM). It is notable that the protease (M^{pro}) inhibitory properties are comparable to the anti-SARS-CoV-2 inhibitory properties presented in Table 1 (IC_{50} ±0.39, 13.53, 8.88 μM for compounds **6b**, **6d** and **6g**, respectively). The slight differences in the results are attributed to differences in the experimental techniques applied (in-vitro and biochemical assays).

2.5. Molecular modeling

Various molecular modeling techniques have been developed over the last decades and are used intensively in medicinal chemical studies for identifying and optimizing the effective hits/leads and determining the parameters controlling biological properties [72,73]. The effective M^{pro}-SARS-CoV-2 agents identified (**6b**, **6d** and **6g**) were used for molecular modeling (docking) studies utilizing PDB ID: 7C8U [74] by Discovery Studio 2.5 software (RMS: 0.088). The standard CDOCKER technique was adopted after protein and ligand optimization (force field: CHARMm, Partial charge: MMFF94, radius of the active site employed: 8.0368 Å) [61]. The results (Fig. 9, Table 3), reveal that compound **6b** is involved in hydrogen bonding interaction of indolyl NH with GLU166 and indolyl Cl with CYS145. The amino acids concerned interact with the co-crystallized ligand in the protein active site (supplementary information file Fig. S60). The high CDOCKER interaction energy score (−52.58 kcal mol^{-1}) is consistent with the higher M^{pro}-SARS-CoV-2 inhibitory properties (IC_{50}=9.605 μM) compared to the other tested analogs. Similar observations have been made for compound **6g** revealing hydrogen bonding interaction of the phosphonate P—O with GLU166 and acceptable docking interaction energy score (−48.823 kcal mol^{-1}) supporting its M^{pro}-SARS-CoV-2 inhibitory properties (IC_{50} = 15.59 μM). Compound **6d** shows hydrogen bonding interaction of piperidinyl nitrogen with GLN189 and phosphonate P—O with GLN189. Although, GLN189 is one of the amino acids of the protein active site, it is not one of the lead amino acids revealing hydrogen bonding interaction with the co-crystallized ligand. These observations explain the low M^{pro}-SARS-CoV-2 inhibitory properties (IC_{50} = 42.82 μM) of **6d** relative to the other tested agents. Thus, the docking studies support the observed M^{pro}-SARS-CoV-2 inhibitory properties and explain the potency of the tested agents based on the presumed mode of action.

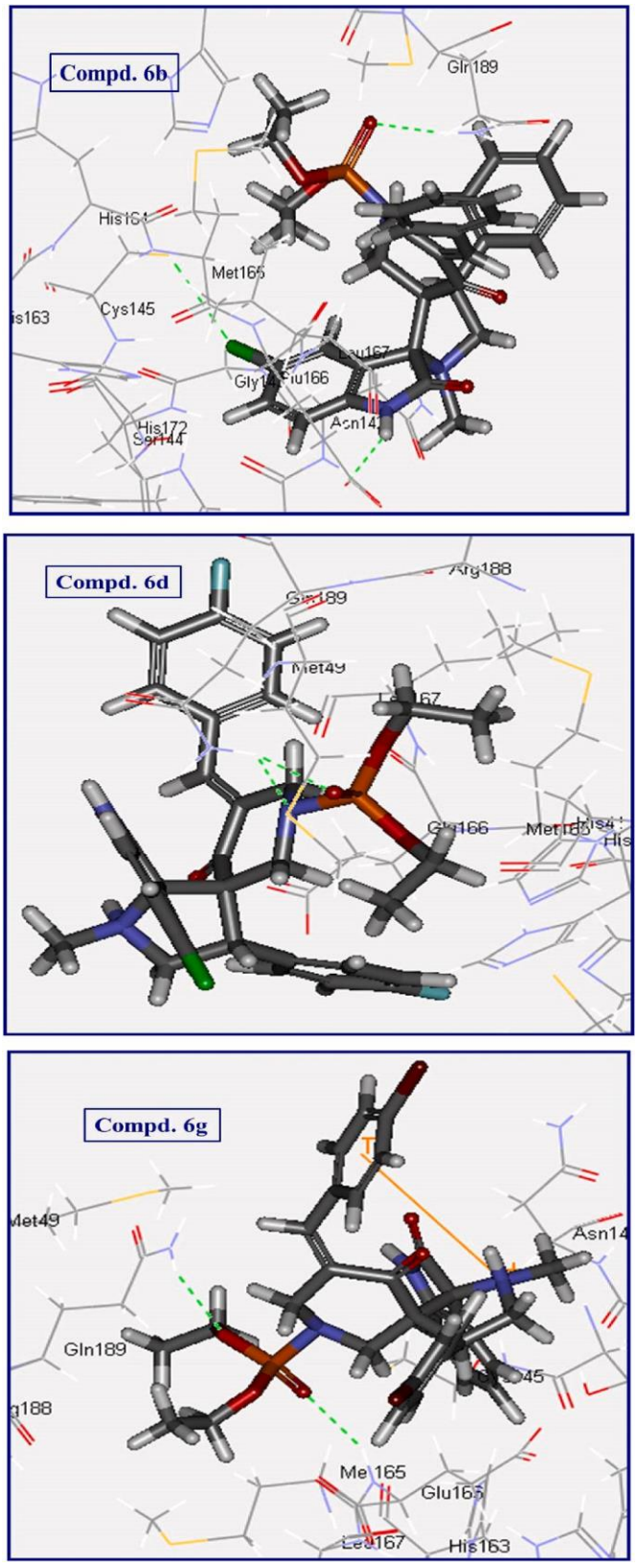

Fig. 9. Docking poses of the spiroindoles (**6b**, **6d** and **6g**) in the active site of PDB ID: 7C8U.

Table 3
Interaction CDOCKER energy scores and hydrogen bonding interactions of the synthesized spiroindoles (**6b**, **6d** and **6g**) in the active site of PDB ID: 7C8U.

Compd.	CDOCKER interaction energy (−Kcal mol^{-1})	Hydrogen bonding interactions
6b	52.58	Phosphonate P—O … GLN189, Indolyl NH … GLU166, Indolyl Cl…CYS145
6d	49.017	Piperidinyl N … GLN189, Phosphonate P—O … GLN189
6g	48.823	Phosphonate P—O … GLU166, Phosphonate OEt …GLN189

3. Conclusion

Spiroindoles **6a–l** bearing the phosphonate group were obtained in excellent yields (80–95%) through microwave-assisted azomethine ylide (produced through interaction of isatins **4** and sarcosine **5**) cycloaddition of *N*-diethyl phosphonate-3,5-bis(ylidene)-4-piperidones **3a–g**. X-ray diffraction studies evidenced the stereochemical configuration. Some of the synthesized spiroindoles revealed potent anti-SARS-CoV-2 properties in the viral infected Vero-E6 cell technique. M^{pro} inhibitory properties were evidenced for the synthesized agents with potent bio-properties by the appropriate Kit assay. Molecular modeling studies (PDB ID: 7C8U) supported the M^{pro}-SARS-CoV-2 inhibitory properties. The observations provide a compelling case for the compounds to be considered in future studies for optimizing potent anti-SARS-CoV-2 agents.

4. Experimental

Melting points were determined on a capillary point apparatus (Stuart SMP3) equipped with a digital thermometer. IR spectra (KBr) were recorded on a Shimadzu FT-IR 8400S spectrophotometer. Reactions were monitored using thin layer chromatography (TLC) on 0.2 mm silica gel F254 plates (Merck) utilizing various solvents for elution. The chemical structures of the synthesized compounds were characterized by nuclear magnetic resonance spectra (^{1}H NMR, ^{13}C NMR) and determined on a Bruker NMR spectrometer (500 MHz, 125 MHz for ^{1}H and ^{13}C, respectively). ^{13}C NMR spectra are fully decoupled. Chemical shifts were reported in parts per million (ppm) using the deuterated solvent peak or tetramethylsilane as an internal standard. Microwave oven used is a Milestone Italy (model: StartSynth, Reactor: Pack2B Basic Single Vessel Kit).

4.1. Chemical synthesis

*4.1.1. Synthesis of diethyl [3,5-di((E)-ylidene)-4-oxopiperidin-1-yl] phosphonates **3a–g** (general procedure)*

To a stirring solution of 3,5-di(*E*)-ylidene)piperidin-4-ones **1a–g** (5 mmol) in DMF (10 ml) containing TEA (triethylamine, 0.8 ml, 6 mmol) in an ice bath (0 °C), diethylchlorophosphate **2** (0.8 ml, 6 mmol) in DMF (10 ml) was added dropwise (within 10 min). The reaction mixture was stirred at the mentioned conditions for 2 h and stored at room temperature (20–25 °C) overnight. After the completion of the reaction (TLC), it was poured into ice-cold water (200 ml) containing NaCl (1.0 g). The separated solid was collected, washed with tap water, dried and crystallized from a suitable solvent affording the corresponding **3a–g**.

*4.1.1.1. Diethyl [3,5-di((E)-benzylidene)-4-oxopiperidin-1-yl]phosphonate (**3a**).* Obtained from the reaction of **1a** and **2**, pale-yellow microcrystals from cyclohexane, mp 134–135 °C (127 °C [75]) and yield 71% (1.45 g). IR: ν_{max}/cm^{-1} 1670, 1612, 1585, 1485, 1261, 1026. ^{1}H NMR (DMSO-d_6) δ (ppm): 1.05 (t, J = 7.1 Hz, 6H, 2 CH_3), 3.75–3.84 (m, 4H, 2 OCH_2), 4.44 (d, J = 9.2 Hz, 4H, 2 NCH_2), 7.45–7.51 (m, 10H, arom. H), 7.73 (s, 2H, 2 olefinic CH). ^{13}C NMR (DMSO-d_6) δ (ppm): 15.67, 15.72 (CH_3), 45.51, 45.54 (NCH_2), 61.80, 61.84 (OCH_2), 128.7, 129.4, 130.3, 133.01, 133.04, 134.3, 135.5 (arom. C + olefinic C), 185.8 (C⁻O). Anal. Calcd. for $C_{23}H_{26}NO_4P$ (411.44): C, 67.14; H, 6.37; N, 3.40. Found: C, 67.26; H, 6.17; N, 3.54.

*4.1.1.2. Diethyl [3,5-bis((E)-4-fluorobenzylidene)-4-oxopiperidin-1-yl] phosphonate (**3b**).* Obtained from the reaction of **1b** and **2**, yellow microcrystals from cyclohexane, mp 112–114 °C and yield 85% (1.9 g). IR: ν_{max}/cm^{-1} 1670, 1601, 1574, 1508, 1443, 1238, 1049. ^{1}H NMR (DMSO-d_6) δ (ppm): 1.07 (t, J = 7.0 Hz, 6H, 2 CH_3), 3.77–3.84 (m, 4H, 2 OCH_2), 4.42 (dd, J = 1.8, 9.2 Hz, 4H, 2 NCH_2), 7.33–7.37 (m, 4H, arom. H), 7.57–7.60 (m, 4H, arom. H), 7.71 (s, 2H, 2 olefinic CH). ^{13}C NMR (DMSO-d_6) δ (ppm): 15.76, 15.81 (CH_3), 45.50, 45.53 (NCH_2), 61.91, 61.95 (OCH_2), 115.8, 116.0, 130.89, 130.91, 132.79, 132.86, 134.4, 161.5, 163.5 (arom. C + olefinic C), 185.7 (C⁻O). Anal. Calcd. for $C_{23}H_{24}F_2NO_4P$ (447.42): C, 61.74; H, 5.41; N, 3.13. Found: C, 61.90; H, 5.12; N, 2.93.

*4.1.1.3. Diethyl [3,5-bis((E)-4-chlorobenzylidene)-4-oxopiperidin-1-yl] phosphonate (**3c**).* Obtained from the reaction of **1c** and **2**, pale yellow microcrystals from cyclohexane, mp 136–137 °C (132 °C [75]) and yield 75% (1.8 g). IR: ν_{max}/cm^{-1} 1678, 1616, 1582, 1489, 1269, 1018. ^{1}H NMR (DMSO-d_6) δ (ppm): 1.05 (t, J = 7.1 Hz, 6H, 2 CH_3), 3.73–3.85 (m, 4H, 2 OCH_2), 4.40 (dd, J = 1.9, 9.3 Hz, 4H, 2 NCH_2), 7.53 (d, J = 8.9 Hz, 4H, arom. H), 7.56 (d, J = 8.9 Hz, 4H, arom. H), 7.68 (s, 2H, 2 olefinic CH). ^{13}C NMR (DMSO-d_6) δ (ppm): 15.79, 15.84 (CH_3), 45.53, 45.56 (NCH_2), 61.95, 61.99 (OCH_2), 128.9, 132.2, 133.2, 133.57, 133.61, 134.2, 134.3 (arom. C + olefinic C), 185.7 (C⁻O). Anal. Calcd. for $C_{23}H_{24}Cl_2NO_4P$ (480.32): C, 57.51; H, 5.04; N, 2.92. Found: C, 57.65; H, 5.10; N, 2.81.

*4.1.1.4. Diethyl [3,5-bis((E)-4-bromobenzylidene)-4-oxopiperidin-1-yl] phosphonate (**3d**).* Obtained from the reaction of **1d** and **2**, pale yellow microcrystals from n-butanol, mp 141–142 °C and yield 74% (2.1 g). IR: ν_{max}/cm^{-1} 1670, 1612, 1585, 1485, 1261, 1022. ^{1}H NMR (DMSO-d_6) δ (ppm): 1.06 (t, J = 7.0 Hz, 6H, 2 CH_3), 3.74–3.86 (m, 4H, 2 OCH_2), 4.40 (d, J = 9.3 Hz, 4H, 2 NCH_2), 7.47 (d, J = 8.4 Hz, 4H, arom. H), 7.67 (s, 2H, 2 olefinic CH), 7.71 (d, J = 8.3 Hz, 4H, arom. H). ^{13}C NMR (DMSO-d_6) δ (ppm): 15.7 (CH_3), 45.4 (NCH_2), 61.9 (OCH_2), 123.0, 131.7, 132.2, 133.4, 133.57, 133.60, 134.3 (arom. C + olefinic C), 185.6 (C⁻O). Anal. Calcd. for $C_{23}H_{24}Br_2NO_4P$ (569.23): C, 48.53; H, 4.25; N, 2.46. Found: C, 48.68; H, 4.37; N, 2.52.

*4.1.1.5. Diethyl [3,5-bis((E)-4-methoxybenzylidene)-4-oxopiperidin-1-yl] phosphonate (**3e**).* Obtained from the reaction of **1e** and **2**, yellow microcrystals from methanol, mp 158–160 °C (144 °C [75]) and yield 81% (1.9 g). IR: ν_{max}/cm^{-1} 1667, 1605, 1578, 1508, 1261, 1026. ^{1}H NMR (DMSO-d_6) δ (ppm): 1.08 (t, J = 7.1 Hz, 6H, 2 CH_3), 3.77–3.86 (m, 10H, 2 OCH_2, 2 OCH_3), 4.42 (d, J 9.0 Hz, 4H, 2 NCH_2), 7.07 (d, J 8.9 Hz, 4H, arom. H), 7.48 (d, J = 8.9 Hz, 4H, arom. H), 7.67 (s, 2H, 2 olefinic CH). ^{13}C NMR (DMSO-d_6) δ (ppm): 15.8, 15.9 (CH_3), 45.66, 45.69 (NCH_2), 55.3 (OCH_3), 61.83, 61.87 (OCH_2), 114.4, 127.0, 131.0, 131.1, 132.5, 135.2, 160.3 (arom. C + olefinic C), 185.5 (C⁻O). Anal. Calcd. for $C_{25}H_{30}NO_6P$ (471.49): C, 63.69; H, 6.41; N, 2.97. Found: C, 63.76; H, 6.55; N, 3.05.

*4.1.1.6. Diethyl [3,5-bis((E)-4-methylbenzylidene)-4-oxopiperidin-1-yl] phosphonate (**3f**).* Obtained from the reaction of **1f** and **2**, pale yellow microcrystals from cyclohexane, mp 158–160 °C (151 °C [75]) and yield 87% (1.9 g). IR: ν_{max}/cm^{-1} 1670, 1609, 1582, 1508, 1261, 1026. ^{1}H NMR (DMSO-d_6) δ (ppm): 1.05 (t, J = 7.0 Hz, 6H, 2 CH_3), 2.36 (s, 6H, 2 $ArCH_3$), 3.74–3.83 (m, 4H, 2 OCH_2), 4.42 (d, J = 9.0 Hz, 4H, 2 NCH_2), 7.31 (d, J = 8.1 Hz, 4H, arom. H), 7.40 (d, J = 8.1 Hz, 4H, arom. H), 7.68 (s, 2H, 2 olefinic CH). ^{13}C NMR (DMSO-d_6) δ (ppm): 15.79, 15.84 (CH_3), 21.0 ($ArCH_3$), 45.6, 45.7 (NCH_2), 61.8, 61.9 (OCH_2), 129.5, 130.5, 131.6, 132.3, 132.4, 135.5, 139.5 (arom. C + olefinic C), 185.7 (C⁻O).

Anal. Calcd. for $C_{25}H_{30}NO_4P$ (439.49): C, 68.32; H, 6.88; N, 3.19. Found: C, 68.50; H, 6.99; N, 3.35.

*4.1.1.7. Diethyl [(3E,5E)-4-oxo-3,5-bis(thiophen-2-ylmethylene)piperidin-1-yl]phosphonate (**3g**).* Obtained from the reaction of **1g** and **2**, buff microcrystals from cyclohexane, mp 123–125 °C and yield 85% (1.8 g). IR: ν_{max}/cm^{-1} 1659, 1593, 1558, 1504, 1443, 1261, 1022. ^{1}H NMR (DMSO-d_6) δ (ppm): 1.16 (t, J = 7.0 Hz, 6H, 2 CH_3), 3.86–3.95 (m, 4H, 2 OCH_2), 4.47 (d, J = 9.3 Hz, 4H, 2 NCH_2), 7.29 (dd, J = 3.7, 5.0 Hz, 2H, arom. H), 7.63 (d, J = 3.4 Hz, 2H, arom. H), 7.89 (s, 2H, 2 olefinic CH), 7.97 (d, J = 5.1 Hz, 2H, arom. H). ^{13}C NMR (DMSO-d_6) δ (ppm): 15.9, 16.0 (CH_3), 45.22, 45.25 (NCH_2), 62.06, 62.10 (OCH_2), 127.8, 128.6, 129.61, 129.64, 132.4, 134.6, 137.5 (arom. C + olefinic C), 184.7 (C=O). Anal. Calcd. for $C_{19}H_{22}NO_4PS_2$ (423.48): C, 53.89; H, 5.24; N, 3.31. Found: C, 53.98; H, 5.38; N, 3.38.

*4.1.2. Synthesis of dispiro[indoline-3,2′-pyrrolidine-3′,3″-piperidin]-1″-yl) phosphonates **6a–l** (general procedure)*

A mixture of equimolar amounts of the appropriate diethyl [3,5-di ((*E*)-ylidene)-4-oxopiperidin-1-yl]phosphonates **3a–g** (1.25 mmol) and the corresponding isatins **4a,b** with sarcosine **5** in ethanol (10 ml) was heated in the microwave reactor at 60 °C (60 Watt) for 60–90 min (hold time). After the completion of the reaction (TLC), the reaction mixture was allowed to cool at room temperature, and the solvent was evaporated under reduced pressure. The separated solid upon triturating the residual material with methanol (5 ml) was collected and crystallized from a suitable solvent affording the corresponding **6a–l**.

*4.1.2.1. Diethyl (E)-(5″-benzylidene-1′-methyl-2,4″-dioxo-4′-phenyldispiro [indoline-3,2′-pyrrolidine-3′,3″-piperidin]-1″-yl)phosphonate (**6a**).* Obtained from the reaction of **3a**, **4a** and **5**, reaction time 90 min as pale yellow microcrystals from ethanol (90%), mp 181–182 °C and yield 92% (0.67 g). IR: ν_{max}/cm^{-1} 3175, 1713, 1674, 1585, 1470, 1227, 1018. ^{1}H NMR (DMSO-d_6) δ (ppm): 0.84 (t, J = 7.0 Hz, 3H, CH_3), 0.98 (t, J = 7.1 Hz, 3H, CH_3), 1.96 (s, 3H, NCH_3), 2.14 (d, J = 13.5 Hz, 1H, upfield H of piperidinyl H_2C-2″), 3.28–3.32 (m, 2H, upfield H of pyrrolidinyl H_2C-5′ + upfield H of piperidinyl H_2C-6″), 3.48–3.88 (m, 7H, downfield H of pyrrolidinyl H_2C-5′ + downfield H of piperidinyl H_2C-2″ + downfield H of piperidinyl H_2C-6″ + 2 OCH_2), 4.71 (t, J = 9.1 Hz, 1H, pyrrolidinyl H-4′), 6.70 (d, J = 7.7 Hz, 1H, arom. H), 6.88–6.92 (m, 2H, arom. H), 7.11–7.15 (m, 3H, arom. H), 7.26 (t, J = 7.3 Hz, 1H, arom. H), 7.33–7.40 (m, 5H, 4 arom. H + olefinic CH), 7.43–7.46 (m, 3H, arom. H), 10.53 (s, 1H, NH). ^{13}C NMR (DMSO-d_6) δ (ppm): 15.56, 15.62, 15.80, 15.81 (CH_3), 33.8 (NCH_3), 45.1 (pyrrolidinyl HC-4′), 46.1 (piperidinyl H_2C-6″), 47.4 (piperidinyl H_2C-2″), 57.1 (pyrrolidinyl H_2C-5′), 61.84, 61.86, 61.88, 61.91, 61.95, 62.03 [spiro-C-3′ (C-3″) + OCH_2], 75.1 [spiro-C-3 (C-2′)], 109.1, 120.9, 125.4, 126.8, 127.0, 128.3, 128.5, 129.0, 129.2, 129.6, 129.8, 131.6, 131.7, 134.2, 137.9, 138.2, 143.7 (arom. C + olefinic C), 175.2, 197.2 (C=O). Anal. Calcd. for $C_{33}H_{36}N_3O_5P$ (585.64): C, 67.68; H, 6.20; N, 7.18. Found: C, 67.85; H, 6.31; N, 7.41.

*4.1.2.2. Diethyl (E)-(5″-benzylidene-5-chloro-1′-methyl-2,4″-dioxo-4′-phenyldispiro[indoline-3,2′-pyrrolidine-3′,3″-piperidin]-1″-yl)phosphonate (**6b**).* Obtained from the reaction of **3a**, **4b** and **5**, reaction time 90 min as buff microcrystals from ethanol (90%), mp 220–221 °C and yield 93% (0.72 g). IR: ν_{max}/cm^{-1} 3175, 3140, 1717, 1682, 1601, 1470, 1238, 1022. ^{1}H NMR (DMSO-d_6) δ (ppm): 0.81 (t, J = 7.0 Hz, 3H, CH_3), 1.00 (t, J = 7.0 Hz, 3H, CH_3), 1.97 (s, 3H, NCH_3), 2.16 (d, J = 13.6 Hz, 1H, upfield H of piperidinyl H_2C-2″), 3.32 (d, J = 8.9 Hz, 1H, upfield H of pyrrolidinyl H_2C-5′), 3.49–3.52 (m, 2H, upfield H of piperidinyl H_2C-6″ + downfield H of pyrrolidinyl H_2C-5′), 3.65–3.90 (m, 6H, downfield H of piperidinyl H_2C-2″ + downfield H of piperidinyl H_2C-6″ + 2 OCH_2), 4.65 (t, J = 8.9 Hz, 1H, pyrrolidinyl H-4′), 6.68 (d, J = 8.3 Hz, 1H, arom. H), 6.82 (s, 1H, arom. H), 7.18–7.21 (m, 3H, arom. H), 7.27 (t, J = 7.3 Hz, 1H, arom. H), 7.34–7.46 (m, 8H, 7 arom. H + olefinic CH), 10.70 (s, 1H, NH). ^{13}C NMR (DMSO-d_6) δ (ppm): 15.47, 15.52, 15.74, 15.79 (CH_3), 33.9 (NCH_3), 45.8 (pyrrolidinyl HC-4′), 46.2 (piperidinyl H_2C-6″), 48.0 (piperidinyl H_2C-2″), 57.4 (pyrrolidinyl H_2C-5′), 61.87, 61.92, 61.96, 62.26, 62.34 [spiro-C-3′ (C-3″) + OCH_2], 75.2 [spiro-C-3 (C-2′)], 110.6, 125.0, 126.7, 127.0, 127.5, 128.3, 128.5, 128.7, 129.3, 129.5, 129.8, 131.7, 131.8, 134.0, 137.9, 142.6 (arom. C + olefinic C), 174.8, 197.2 (C=O). Anal. Calcd. for $C_{33}H_{35}ClN_3O_5P$ (620.08): C, 63.92; H, 5.69; N, 6.78. Found: C, 63.86; H, 5.78; N, 6.86.

*4.1.2.3. Diethyl (E)-[5″-(4-fluorobenzylidene)-4′-(4-fluorophenyl)-1′-methyl-2,4″-dioxodispiro[indoline-3,2′-pyrrolidine-3′,3″-piperidin]-1″-yl] phosphonate (**6c**).* Obtained from the reaction of **3b**, **4a** and **5**, reaction time 60 min as pale yellow microcrystals from methanol, mp 193–194 °C and yield 94% (0.73 g). IR: ν_{max}/cm^{-1} 3186, 1705, 1682, 1601, 1508, 1223, 1030. ^{1}H NMR (DMSO-d_6) δ (ppm): 0.85 (t, J = 7.1 Hz, 3H, CH_3), 1.00 (t, J = 7.0 Hz, 3H, CH_3), 1.94 (s, 3H, NCH_3), 2.17 (d, J = 13.4 Hz, 1H, upfield H of piperidinyl H_2C-2″), 3.27–3.28 (m, 1H, upfield H of pyrrolidinyl H_2C-5′) 3.32 (d, J = 8.4 Hz, 1H, upfield H of piperidinyl H_2C-6″), 3.49–3.81 (m, 7H, downfield H of pyrrolidinyl H_2C-5′ + downfield H of piperidinyl H_2C-2″ + downfield H of piperidinyl H_2C-6″ + 2 OCH_2), 4.66 (dd, J = 8.1, 10.0 Hz, 1H, pyrrolidinyl H-4′), 6.69 (d, J = 7.7 Hz, 1H, arom. H), 6.88–6.90 (m, 2H, arom. H), 7.11–7.27 (m, 7H, arom. H), 7.41 (s, 1H, olefinic CH), 7.50 (dd, J = 5.6, 8.5 Hz, 2H, arom. H), 10.56 (s, 1H, NH). ^{13}C NMR (DMSO-d_6) δ (ppm): 15.6, 15.7, 15.8, 15.9 (CH_3), 33.9 (NCH_3), 45.2 (pyrrolidinyl HC-4′), 45.4 (piperidinyl H_2C-6″), 47.4 (piperidinyl H_2C-2″), 57.6 (pyrrolidinyl H_2C-5′), 61.7, 61.8, 61.91, 61.95, 61.99 [spiro-C-3′ (C-3″) + OCH_2], 75.3 [spiro-C-3 (C-2′)], 109.2, 115.0, 115.1, 115.6, 115.8, 121.0, 125.2, 126.9, 129.1, 130.69, 130.72, 131.4, 131.76, 131.82, 132.08, 132.15, 134.39, 134.41, 136.8, 143.6, 160.3, 161.3, 162.2, 163.2 (arom. C + olefinic C), 175.3, 197.2 (C=O). Anal. Calcd. for $C_{33}H_{34}F_2N_3O_5P$ (621.62): C, 63.76; H, 5.51; N, 6.76. Found: C, 63.52; H, 5.34; N, 6.57.

***4.1.2.4.** Diethyl (E)-[5-chloro-5″-(4-fluorobenzylidene)-4′-(4-fluorophenyl)-1′-methyl-2,4″-dioxodispiro[indoline-3,2′-pyrrolidine-3′,3″-piperidin]-1″-yl]phosphonate (**6d**).* Obtained from the reaction of **3b**, **4b** and **5**, reaction time 60 min as pale yellow microcrystals from n-butanol, mp 234–235 °C and yield 93% (0.76 g). IR: ν_{max}/cm^{-1} 3183, 1713, 1682, 1601, 1508, 1227, 1026. ^{1}H NMR (DMSO-d_6) δ (ppm): 0.82 (t, J = 7.0 Hz, 3H, CH_3), 1.01 (t, J = 7.0 Hz, 3H, CH_3), 1.94 (s, 3H, NCH_3), 2.18 (d, J = 13.5 Hz, 1H, upfield H of piperidinyl H_2C-2″), 3.34 (t, J = 8.5 Hz, 1H, upfield H of pyrrolidinyl H_2C-5′), 3.44–3.82 (m, 8H, upfield H of piperidinyl H_2C-6″ + downfield H of pyrrolidinyl H_2C-5′ + downfield H of piperidinyl H_2C-2″ + downfield H of piperidinyl H_2C-6″ + 2 OCH_2), 4.61 (dd, J = 8.1, 9.9 Hz, 1H, pyrrolidinyl H-4′), 6.67 (d, J = 8.4 Hz, 1H, arom. H), 6.79 (d, J = 2.2 Hz, 1H, arom. H), 7.18 (dt, J = 1.9, 8.9 Hz, 3H, arom. H), 7.23–7.30 (m, 4H, arom. H), 7.39 (s, 1H, olefinic CH), 7.49 (dd, J = 5.5, 8.5 Hz, 2H, arom. H), 10.72 (s, 1H, NH). ^{13}C NMR (DMSO-d_6) δ (ppm): 15.59, 15.64, 15.86, 15.90 (CH_3), 33.9 (NCH_3), 45.6 (pyrrolidinyl HC-4′), 45.9 (piperidinyl H_2C-6″), 48.0 (piperidinyl H_2C-2″), 57.9 (pyrrolidinyl H_2C-5′), 62.00, 62.05, 62.07, 62.10, 62.15 [spiro-C-3′ (C-3″) + OCH_2], 75.4 [spiro-C-3 (C-2′)], 110.7, 115.0,115.2, 115.7, 115.9, 125.0, 126.7, 127.5, 128.9, 130.54, 130.57, 131.7, 131.8, 131.9, 132.1, 132.2, 134.19, 134.21, 136.9, 142.6, 160.3, 161.4, 162.3, 163.3 (arom. C + olefinic C), 175.0, 197.1 (C=O). Anal. Calcd. for $C_{33}H_{33}ClF_2N_3O_5P$ (656.06): C, 60.42; H, 5.07; N, 6.41. Found: C, 60.29; H, 5.13; N, 6.28.

*4.1.2.5. Diethyl (E)-[5″-(4-chlorobenzylidene)-4′-(4-chlorophenyl)-1′-methyl-2,4″-dioxodispiro[indoline-3,2′-pyrrolidine-3′,3″-piperidin]-1″-yl] phosphonate (**6e**).* Obtained from the reaction of **3c**, **4a** and **5**, reaction time 60 min as pale yellow microcrystals from benzene − light petroleum as 1:2 v/v, mp 143–145 °C and yield 91% (0.74 g). IR: ν_{max}/cm^{-1} 3260, 1713, 1682, 1605, 1489, 1227, 1015. ^{1}H NMR (DMSO-d_6) δ (ppm): 0.84 (t, J = 7.1 Hz, 3H, CH_3), 0.99 (t, J = 7.0 Hz, 3H, CH_3), 1.92

(s, 3H, NCH_3), 2.18 (d, J = 13.5 Hz, 1H, upfield H of piperidinyl H_2C-2′′), 3.27–3.33 (m, 2H, upfield H of pyrrolidinyl H_2C-5′ + upfield H of piperidinyl H_2C-6′′), 3.46–3.81 (m, 7H, downfield H of pyrrolidinyl H_2C-5′ + downfield H of piperidinyl H_2C-2′′ + downfield H of piperidinyl H_2C-6′′ + 2 OCH_2), 4.64 (t, J = 9.0 Hz, 1H, pyrrolidinyl H-4′), 6.67 (d, J 7.8 Hz, 1H, arom. H), 6.87–6.91 (m, 2H, arom. H), 7.10–7.15 (m, 3H, arom. H), 7.39 (d, J = 7.0 Hz, 2H, arom. H), 7.41 (s, 1H, olefinic CH), 7.46 (d, J = 8.6 Hz, 2H, arom. H), 7.48 (d, J = 8.3 Hz, 2H, arom. H), 10.58 (s, 1H, NH). ^{13}C NMR (DMSO-d_6) δ (ppm): 15.6, 15.7, 15.84, 15.88 (CH_3), 33.9 (NCH_3), 45.2 (pyrrolidinyl HC-4′), 45.6 (piperidinyl H_2C-6′′), 47.4 (piperidinyl H_2C-2′′), 57.4 (pyrrolidinyl H_2C-5′), 61.8, 61.88, 61.95, 61.98, 62.00, 62.03 [spiro-C-3′ (C-3′′) + OCH_2], 75.3 [spiro-C-3 (C-2′)], 109.3, 121.0, 125.2, 126.9, 128.3, 128.7, 129.1, 131.4, 131.7, 131.8, 132.15, 132.23, 133.0, 134.0, 136.5, 137.3, 143.6 (arom. C + olefinic C), 175.3, 197.1 (C=O). Anal. Calcd. for $C_{33}H_{34}Cl_2N_3O_5P$ (654.52): C, 60.56; H, 5.24; N, 6.42. Found: C, 60.66; H, 5.42; N, 6.61.

*4.1.2.6. Diethyl (E)-[5-chloro-5′′-(4-chlorobenzylidene)-4′-(4-chlorophenyl)-1′-methyl-2,4′′-dioxodispiro[indoline-3,2′-pyrrolidine-3′,3′′-piperidin]-1′′-yl]phosphonate (**6f**).* Obtained from the reaction of **3c**, **4b** and **5**, reaction time 60 min as pale yellow microcrystals from methanol, mp 229–230 °C and yield 88% (0.76 g). IR: ν_{max}/cm^{-1} 3175, 3140, 1713, 1682, 1605, 1493, 1238, 1026. ^{1}H NMR (DMSO-d_6) δ (ppm): 0.84 (t, J = 7.1 Hz, 3H, CH_3), 1.02 (t, J = 7.0 Hz, 3H, CH_3), 1.95 (s, 3H, NCH_3), 2.22 (d, J = 13.5 Hz, 1H, upfield H of piperidinyl H_2C-2′′), 3.35 (t, J = 8.4 Hz, 1H, upfield H of pyrrolidinyl H_2C-5′), 3.45–3.81 (m, 8H, upfield H of piperidinyl H_2C-6′′ + downfield H of pyrrolidinyl H_2C-5′ + downfield H of piperidinyl H_2C-2′′ + downfield H of piperidinyl H_2C-6′′ + 2 OCH_2), 4.61 (dd, J = 8.1, 9.9 Hz, 1H, pyrrolidinyl H-4′), 6.69 (d, J = 8.3 Hz, 1H, arom. H), 6.79 (d, J = 2.2 Hz, 1H, arom. H), 7.19–7.22 (m, 3H, arom. H), 7.37–7.52 (m, 7H, arom. H + olefinic CH), 10.74 (s, 1H, NH). ^{13}C NMR (DMSO-d_6) δ (ppm): 15.62, 15.67, 15.85, 15.90 (CH_3), 33.9 (NCH_3), 45.7 (pyrrolidinyl HC-4′), 45.8 (piperidinyl H_2C-6′′), 47.9 (piperidinyl H_2C-2′′), 57.7 (pyrrolidinyl H_2C-5′), 62.0, 62.08, 62.13, 62.15, 62.22 [spiro-C-3′ (C-3′′) + OCH_2), 75.4 [spiro-C-3 (C-2′)], 110.8, 125.0, 126.8, 127.4, 128.3, 128.8, 128.9, 131.4, 131.8, 131.9, 132.3, 132.4, 132.9, 134.2, 136.5, 137.1, 142.6 (arom. C + olefinic C), 175.9, 197.0 (C=O). Anal. Calcd. for $C_{33}H_{33}Cl_3N_3O_5P$ (688.97): C, 57.53; H, 4.83; N, 6.10. Found: C, 57.69; H, 5.15; N, 6.21.

*4.1.2.7. Diethyl (E)-[5′′-(4-bromobenzylidene)-4′-(4-bromophenyl)-1′-methyl-2,4′′-dioxodispiro[indoline-3,2′-pyrrolidine-3′,3′′-piperidin]-1′′-yl] phosphonate (**6g**).* Obtained from the reaction of **3d**, **4a** and **5**, reaction time 60 min as pale yellow microcrystals from methanol, mp 137–139 °C and yield 85% (0.79 g). IR: ν_{max}/cm^{-1} 3167, 1709, 1686, 1616, 1597, 1238, 1022. ^{1}H NMR (DMSO-d_6) δ (ppm): 0.85 (t, J = 7.0 Hz, 3H, CH_3), 1.01 (t, J = 7.1 Hz, 3H, CH_3), 1.93 (s, 3H, NCH_3), 2.20 (d, J = 13.4 Hz, 1H, upfield H of piperidinyl H_2C-2′′), 3.28–3.32 (m, 1H, upfield H of pyrrolidinyl H_2C-5′) 3.49–3.80 (m, 8H, upfield H of piperidinyl H_2C-6′′ + downfield H of pyrrolidinyl H_2C-5′ + downfield H of piperidinyl H_2C-2′′ + downfield H of piperidinyl H_2C-6′′ + 2 OCH_2), 4.63 (dd, J = 8.1, 9.9 Hz, 1H, pyrrolidinyl H-4′), 6.68 (d, J = 7.8 Hz, 1H, arom. H), 6.86–6.90 (m, 2H, arom. H), 7.08 (dd, J = 2.1, 6.5 Hz, 2H, arom. H), 7.13 (dt, J = 2.3, 7.3 Hz, 1H, arom. H), 7.36 (s, 1H, olefinic CH), 7.42 (d, J = 8.2 Hz, 2H, arom. H), 7.55 (d, J = 8.2 Hz, 2H, arom. H), 7.61 (dd, J = 2.0, 6.5 Hz, 2H, arom. H), 10.58 (s, 1H, NH). ^{13}C NMR (DMSO-d_6) δ (ppm): 15.6, 15.7, 15.8, 15.9 (CH_3), 33.9 (NCH_3), 45.2 (pyrrolidinyl HC-4′), 45.6 (piperidinyl H_2C-6′′), 47.4 (piperidinyl H_2C-2′′), 57.3 (pyrrolidinyl H_2C-5′), 61.8, 61.9, 61.95, 61.99, 62.0 [spiro-C-3′ (C-3′′) + OCH_2], 75.3 [spiro-C-3 (C-2′)], 109.3, 120.2, 121.0, 122.8, 125.1, 126.9, 129.1, 131.2, 131.58, 131.63, 132.2, 133.4, 136.6, 137.7, 143.6 (arom. C + olefinic C), 175.3, 197.1 (C=O). Anal. Calcd. for $C_{33}H_{34}Br_2N_3O_5P$ (743.43): C, 53.32; H, 4.61; N, 5.65. Found: C, 53.51; H, 4.77; N, 5.73.

*4.1.2.8. Diethyl (E)-[5′′-(4-methoxybenzylidene)-4′-(4-methoxyphenyl)-1′-methyl-2,4′′-dioxodispiro[indoline-3,2′-pyrrolidine-3′,3′′-piperidin]-1′′-yl]phosphonate (**6h**).* Obtained from the reaction of **3e**, **4a** and **5**, reaction time 60 min as pale yellow microcrystals from methanol, mp 196–198 °C and yield 93% (0.75 g). IR: ν_{max}/cm^{-1} 3171, 1705, 1682, 1593, 1512, 1258, 1026. ^{1}H NMR (DMSO-d_6) δ (ppm): 0.90 (t, J = 7.1 Hz, 3H, CH_3), 1.01 (t, J = 7.0 Hz, 3H, CH_3), 1.92 (s, 3H, NCH_3), 2.13 (d, J = 13.5 Hz, 1H, upfield H of piperidinyl H_2C-2′′), 3.23–3.28 (m, 2H, upfield H of pyrrolidinyl H_2C-5′ + upfield H of piperidinyl H_2C-6′′), 3.52–3.82 (m, 13H, downfield H of pyrrolidinyl H_2C-5′ + downfield H of piperidinyl H_2C-2′′ + downfield H of piperidinyl H_2C-6′′ + 2 OCH_2 + 2OCH_3), 4.62 (t, J = 9.1 Hz, 1H, pyrrolidinyl H-4′), 6.67 (d, J = 7.7 Hz, 1H, arom. H), 6.81–6.86 (m, 2H, arom. H), 6.89 (d, J = 9.0 Hz, 2H, arom. H), 6.96 (d, J = 9.0 Hz, 2H, arom. H), 7.11 (d, J = 8.8 Hz, 2H, arom. H), 7.34–7.36 (m, 3H, arom. H), 7.42 (s, 1H, olefinic CH), 10.52 (s, 1H, NH). ^{13}C NMR (DMSO-d_6) δ (ppm): 15.72, 15.77, 15.86, 15.90 (CH_3), 33.9 (NCH_3), 45.2 (pyrrolidinyl HC-4′), 45.4 (piperidinyl H_2C-6′′), 47.1 (piperidinyl H_2C-2′′), 55.0, 55.3 (OCH_3), 57.4 (pyrrolidinyl H_2C-5′), 61.65, 61.73, 61.88, 61.93 [spiro-C-3′ (C-3′′) + OCH_2], 75.2 [spiro-C-3 (C-2′)], 109.1, 113.7, 114.2, 120.8, 125.5, 126.6, 126.8, 128.3, 128.9, 129.3, 129.4, 130.1, 130.9, 132.0, 137.8, 143.7, 158.2, 160.1 (arom. C + olefinic C), 175.3, 197.1 (C=O). Anal. Calcd. for $C_{35}H_{40}N_3O_7P$ (645.69): C, 65.11; H, 6.24; N, 6.51. Found: C, 65.19; H, 6.28; N, 6.68.

*4.1.2.9. Diethyl (E)-[1′-methyl-5′′-(4-methylbenzylidene)-2,4′′-dioxo-4′-(p-tolyl)dispiro[indoline-3,2′-pyrrolidine-3′,3′′-piperidin]-1′′-yl]phosphonate (**6i**).* Obtained from the reaction of **3f**, **4a** and **5**, reaction time 70 min as pale yellow microcrystals from methanol, mp 226–227 °C and yield 95% (0.73 g). IR: ν_{max}/cm^{-1} 3179, 1713, 1678, 1620, 1589, 1261, 1022. ^{1}H NMR (DMSO-d_6) δ (ppm): 0.87 (t, J = 7.1 Hz, 3H, CH_3), 0.99 (t, J = 7.1 Hz, 3H, CH_3), 1.93 (s, 3H, NCH_3), 2.12 (d, J = 13.4 Hz, 1H, upfield H of piperidinyl H_2C-2′′), 2.27 (s, 3H, $ArCH_3$), 2.28 (s, 3H, $ArCH_3$), 3.23–3.29 (m, 2H, upfield H of pyrrolidinyl H_2C-5′ + upfield H of piperidinyl H_2C-6′′), 3.50–3.84 (m, 7H, downfield H of pyrrolidinyl H_2C-5′ + downfield H of piperidinyl H_2C-2′′ + downfield H of piperidinyl H_2C-6′′ + 2 OCH_2), 4.63 (t, J = 9.2 Hz, 1H, pyrrolidinyl H-4′), 6.67 (d, J = 8.4 Hz, 1H, arom. H), 6.85–6.87 (m, 2H, arom. H), 7.01 (d, J = 8.3 Hz, 2H, arom. H), 7.09–7.14 (m, 3H, arom. H), 7.19 (d, J = 8.1 Hz, 2H, arom. H), 7.31 (d, J = 8.3 Hz, 2H, arom. H), 7.39 (s, 1H, olefinic CH), 10.51 (s, 1H, NH). ^{13}C NMR (DMSO-d_6) δ (ppm): 15.68, 15.73, 15.8, 15.9 (CH_3), 20.7, 20.9 ($ArCH_3$), 33.9 (NCH_3), 45.1 (pyrrolidinyl HC-4′), 45.7 (piperidinyl H_2C-6′′), 47.3 (piperidinyl H_2C-2′′), 57.2 (pyrrolidinyl H_2C-5′), 61.8, 61.90, 61.94, 61.96 [spiro-C-3′ (C-3′′), + OCH_2], 75.1 [spiro-C-3 (C-2′)], 109.1, 120.9, 125.5, 126.8, 128.9, 129.0, 129.2, 129.7, 129.9, 130.7, 130.8, 131.4, 135.1, 136.0, 137.9, 139.3, 143.7 (arom. C + olefinic C), 175.3, 197.2 (C=O). Anal. Calcd. for $C_{35}H_{40}N_3O_5P$ (613.69): C, 68.50; H, 6.57; N, 6.85. Found: C, 68.71; H, 6.70; N, 6.91.

*4.1.2.10. Diethyl (E)-[5-chloro-1′-methyl-5′′-(4-methylbenzylidene)-2,4′′-dioxo-4′-(p-tolyl)dispiro[indoline-3,2′-pyrrolidine-3′,3′′-piperidin]-1′′-yl] phosphonate (**6j**).* Obtained from the reaction of **3f**, **4b** and **5**, reaction time 60 min as pale yellow microcrystals from ethyl acetate, mp 227–228 °C and yield 93% (0.75 g). IR: ν_{max}/cm^{-1} 3175, 3140, 1717, 1682, 1597, 1512, 1238, 1026. ^{1}H NMR (DMSO-d_6) δ (ppm): 0.86 (t, J = 7.1 Hz, 3H, CH_3), 1.02 (t, J = 7.0 Hz, 3H, CH_3), 1.95 (s, 3H, NCH_3), 2.15 (d, J = 13.6 Hz, 1H, upfield H of piperidinyl H_2C-2′′), 2.29 (s, 3H, $ArCH_3$), 2.30 (s, 3H, $ArCH_3$), 3.28 (t, J = 8.4 Hz, 1H, upfield H of pyrrolidinyl H_2C-5′), 3.47–3.86 (m, 8H, upfield H of piperidinyl H_2C-6′′ + downfield H of pyrrolidinyl H_2C-5′ + downfield H of piperidinyl H_2C-2′′ + downfield H of piperidinyl H_2C-6′′ + 2 OCH_2), 4.60 (dd, J = 8.0, 10.1 Hz, 1H, pyrrolidinyl H-4′), 6.67 (d, J = 8.3 Hz, 1H, arom. H), 6.80 (d, J = 2.3 Hz, 1H, arom. H), 7.09 (d, J = 7.9 Hz, 2H, arom. H), 7.16 (d, J = 7.8 Hz, 2H, arom. H), 7.18 (dd, J = 2.2, 8.3 Hz, 1H, arom. H), 7.23 (d,

J ≠.9 Hz, 2H, arom. H), 7.32 (d, J ≠.7 Hz, 2H, arom. H), 7.38 (s, 1H, olefinic CH), 10.68 (s, 1H, NH). ^{13}C NMR (DMSO-d_6) δ (ppm): 15.64, 15.69, 15.84, 15.89 (CH_3), 20.7, 20.9 ($ArCH_3$), 34.0 (NCH_3), 45.9 (pyrrolidinyl HC-4′ + piperidinyl H_2C-6″), 47.9 (piperidinyl H_2C-2″), 57.5 (pyrrolidinyl H_2C-5′), 62.00, 62.02, 62.07, 62.19, 62.27 [spiro-C-3′ (C-3″) +OCH_2), 75.3 [spiro-C-3 (C-2′)], 110.6, 125.0, 126.7, 127.7, 128.8, 129.0, 129.3, 129.8, 129.9, 130.9, 131.0, 131.2, 134.9, 136.1, 138.1, 139.5, 142.6 (arom. C + olefinic C), 174.9, 197.3 (C⁻O). Anal. Calcd. for $C_{35}H_{39}ClN_3O_5P$ (648.14): C, 64.86; H, 6.07; N, 6.48. Found: C, 64.97; H, 6.19; N, 6.66.

*4.1.2.11. Diethyl (E)-[1′-methyl-2,4″-dioxo-4′-(thiophen-2-yl)-5″-(thiophen-2-ylmethylene)dispiro[indoline-3,2′-pyrrolidine-3′,3″-piperidin]-1″-yl]phosphonate (**6k**).* Obtained from the reaction of **3g**, **4a** and **5**, reaction time 60 min as pale yellow microcrystals from methanol, mp 206–208 °C and yield 83% (0.62 g). IR: ν_{max}/cm^{-1} 3186, 1709, 1674, 1616, 1570, 1238, 1026. ^{1}H NMR (DMSO-d_6) δ (ppm): 1.06 (t, J = 7.0 Hz, 3H, CH_3), 1.10 (t, J = 7.0 Hz, 3H, CH_3), 1.92 (s, 3H, NCH_3), 2.40 (d, J = 13.4 Hz, 1H, upfield H of piperidinyl H_2C-2″), 3.28 (d, J = 16.1 Hz, 1H, upfield H of piperidinyl H_2C-6″) 3.39 (t, J = 8.4 Hz, 1H, upfield H of pyrrolidinyl H_2C-5′), 3.64–3.97 (m, 7H, downfield H of pyrrolidinyl H_2C-5′ + downfield H of piperidinyl H_2C-2″ + downfield H of piperidinyl H_2C-6″ + 2 OCH_2), 4.89 (dd, J = 8.1, 9.9 Hz, 1H, pyrrolidinyl H-4′), 6.68–6.73 (m, 2H, arom. H), 6.80 (dd, J=1.4, 7.7 Hz, 1H, arom. H), 7.02 (dd, J = 3.4, 5.2 Hz, 1H, arom. H), 7.08 (dt, J = 1.4, 7.6 Hz, 1H, arom. H), 7.12 (dd, J = 1.2, 3.6 Hz, 1H, arom. H), 7.24 (dd, J = 3.7, 5.1 Hz, 1H, arom. H), 7.41 (dd, J = 1.2, 5.2 Hz, 1H, arom. H), 7.54 (d, J = 3.7 Hz, 1H, arom. H), 7.83 (d, J = 2.0 Hz, 1H, olefinic CH), 7.91 (d, J = 5.1 Hz, 1H, arom. H), 10.56 (s, 1H, NH). ^{13}C NMR (DMSO-d_6) δ (ppm): 15.93, 15.97, 15.99, 16.01 (CH_3), 33.7 (NCH_3), 40.7 (pyrrolidinyl HC-4′), 45.4 (piperidinyl H_2C-6″), 46.0 (piperidinyl H_2C-2″), 58.3 (pyrrolidinyl H_2C-5′), 61.06, 61.14, 61.95, 62.0, 62.05, 62.09 [spiro-C-3′ (C-3″) + OCH_2], 75.1 [spiro-C-3 (C-2′)], 109.2, 120.7, 125.0, 125.1, 126.4, 126.76, 126.85, 127.07, 127.2, 128.4, 129.0, 130.3, 133.1, 135.2, 137.1, 140.9, 143.8 (arom. C + olefinic C), 175.0, 195.6 (C⁻O). Anal. Calcd. for $C_{29}H_{32}N_3O_5PS_2$ (597.68): C, 58.28; H, 5.40; N, 7.03. Found: C, 58.42; H, 5.46; N, 6.84.

*4.1.2.12. Diethyl (E)-[5-chloro-1′-methyl-2,4″-dioxo-4′-(thiophen-2-yl)-5″-(thiophen-2-ylmethylene)dispiro[indoline-3,2′-pyrrolidine-3′,3″-piperidin]-1″-yl]phosphonate (**6l**).* Obtained from the reaction of **3g**, **4b** and **5**, reaction time 60 min as pale yellow microcrystals from methanol, mp 223–225 °C and yield 80% (0.63 g). IR: ν_{max}/cm^{-1} 3179, 3140, 1717, 1678, 1616, 1578, 1242, 1026. ^{1}H NMR (DMSO-d_6) δ (ppm): 1.06 (t, J = 7.0 Hz, 3H, CH_3), 1.10 (t, J = 7.0 Hz, 3H, CH_3), 1.93 (s, 3H, NCH_3), 2.42 (d, J = 13.6 Hz, 1H, upfield H of piperidinyl H_2C-2″), 3.41 (t, J = 8.4 Hz, 1H, upfield H of pyrrolidinyl H_2C-5′) 3.45 (d, J = 15.3 Hz, 1H, upfield H of piperidinyl H_2C-6″), 3.64–3.95 (m, 7H, downfield H of pyrrolidinyl H_2C-5′ + downfield H of piperidinyl H_2C-2″ + downfield H of piperidinyl H_2C-6″ + 2 OCH_2), 4.85 (t, J = 9.0 Hz, 1H, pyrrolidinyl H-4′), 6.67 (d, J = 8.3 Hz, 1H, arom. H), 6.72 (d, J=2.3 Hz, 1H, arom. H), 7.01 (dd, J = 3.4, 5.1 Hz, 1H, arom. H), 7.11 (d, J = 3.5 Hz, 1H, arom. H), 7.13 (dd, J = 2.3, 8.3 Hz, 1H, arom. H), 7.25 (dd, J = 3.7, 5.1 Hz, 1H, arom. H), 7.41 (dd, J = 1.3, 5.1 Hz, 1H, arom. H), 7.54 (d, J = 3.3 Hz, 1H, arom. H), 7.82 (s, 1H, olefinic CH), 7.93 (d, J = 5.1 Hz, 1H, arom. H), 10.70 (s, 1H, NH). ^{13}C NMR (DMSO-d_6) δ (ppm): 15.94, 15.98, 15.99, 16.02 (CH_3), 33.8 (NCH_3), 40.7 (piperidinyl H_2C-2″), 45.8 (pyrrolidinyl HC-4′), 46.3 (piperidinyl H_2C-6″), 58.6 (pyrrolidinyl H_2C-5′), 61.4, 61.5 [spiro-C-3′ (C-3″)], 62.03, 62.08, 62.15, 62.20 (OCH_2), 75.2 [spiro-C-3 (C-2′)], 110.6, 124.96, 125.1, 126.5, 126.86, 126.95, 127.1, 127.2, 127.3, 128.5, 128.8, 130.5, 133.3, 135.2, 137.0, 140.7, 142.7 (arom. C + olefinic C), 174.7, 195.6 (C⁻O). Anal. Calcd. for $C_{29}H_{31}ClN_3O_5PS_2$ (632.13): C, 55.10; H, 4.94; N, 6.65. Found: C, 55.29; H, 4.99; N, 6.72.

4.2. X-ray, biological and computational studies

Described in the supplementary information.

Declaration of competing interest

The authors declare that they have no known competing financial interests or personal relationships that could have appeared to influence the work reported in this paper.

Data availability

No data was used for the research described in the article.

Acknowledgment

This work was supported financially by National Research Centre, Egypt, project ID: 13060103.

Appendix A. Supplementary data

Supplementary data to this article can be found online at https://doi.org/10.1016/j.ejmech.2023.115563.

References

[1] J.M. Sanders, M.L. Monogue, T.Z. Jodlowski, J.B. Cutrell, Pharmacologic treatments for coronavirus disease 2019 (COVID-19) A Review, JAMA 323 (2020) 1824–1836. https://doi:10.1001/jama.2020.6019.

[2] L. Zheng, L. Zhang, J. Huang, K.S. Nandakumar, S. Liu, K. Cheng, Potential treatment methods targeting 2019-nCoV infection, Eur. J. Med. Chem. 205 (2020), 112687, https://doi.org/10.1016/j.ejmech.2020.112687.

[3] P. Zhou, X.-L. Yang, X.-G. Wang, B. Hu, L. Zhang, W. Zhang, H.-R. Si, Y. Zhu, B. Li, C.-L. Huang, H.-D. Chen, J. Chen, Y. Luo, H. Guo, R.-D. Jiang, M.-Q. Liu, Y. Chen, X.-R. Shen, X. Wang, X.-S. Zheng, K. Zhao, Q.-J. Chen, F. Deng, L.-L. Liu, B. Yan, F.-X. Zhan, Y.-Y. Wang, G.-F. Xiao, Z.-L. Shi, A pneumonia outbreak associated with a new coronavirus of probable bat origin, Nature 579 (2020) 270–273, https://doi.org/10.1038/s41586-020-2012-7.

[4] L. Buonaguro, M. Tagliamonte, M.L. Tornesello, F.M. Buonaguro, SARS-CoV-2 RNA polymerase as target for antiviral therapy, J. Transl. Med. 18 (2020) 185, https://doi.org/10.1186/s12967-020-02355-3.

[5] S. Durmuş, K.Ö. Ülgen, Comparative interactomics for virus-human protein-protein interactions: DNA viruses versus RNA viruses, FEBS Open Bio 7 (2017) 96–107. https://doi:10.1002/2211-5463.12167.

[6] W. Zhu, C.Z. Chen, K. Gorshkov, M. Xu, D.C. Lo, W. Zheng, RNA-dependent RNA polymerase as a target for COVID-19 drug discovery, SLAS Discovery 25 (2020) 1141–1151, https://doi.org/10.1177/24725552209421.

[7] K. Dhama, S.K. Patel, K. Sharun, M. Pathak, R. Tiwari, M.I. Yatoo, Y.S. Malik, R. Sah, A.A. Rabaan, P.K. Panwar, K.P. Singh, I. Michalak, W. Chaicumpa, D. F. Martinez-Pulgarin, D.K. Bonilla-Aldana, A.J. Rodriguez-Morales, SARS-CoV-2 jumping the species barrier: zoonotic lessons from SARS, MERS and recent advances to combat this pandemic virus, Trav. Med. Infect. Dis. 37 (2020), 101830, https://doi.org/10.1016/j.tmaid.2020.101830.

[8] https://covid19.who.int/. (Accessed 1 April 2023).

[9] K. Jayabal, D. Elumalai, S. Leelakrishnan, S. Bhattacharya, V. Rengarajan, T. Kannan, S.-C. Chuang, Green and regioselective approach for the synthesis of 3-substituted indole based 1,2-dihydropyridine and azaxanthone derivatives as a potential lead for SARS-CoV-2 and delta plus mutant virus: DFT and docking studies, ACS Omega 7 (2022) 43856–43876, https://doi.org/10.1021/acsomega.2c04990.

[10] T. Barhoumi, B. Alghanem, H. Shaibah, F.A. Mansour, H.S. Alamri, M.A. Akiel, F. Alroqi, M. Boudjelal, SARS-CoV-2 coronavirus spike protein-induced apoptosis, inflammatory, and oxidative stress responses in THP-1-like-macrophages: potential role of angiotensin-converting enzyme inhibitor (perindopril), Front. Immunol. 12 (2021), 728896. https://doi:10.3389/fimmu.2021.728896.

[11] https://www.who.int/activities/tracking-SARS-CoV-2-variants/. (Accessed 1 April 2023).

[12] https://www.cdc.gov/coronavirus/2019-ncov/variants/variant-classifications.html. (Accessed 1 April 2023).

[13] Y. Araf, F. Akter, Y.-d. Tang, R. Fatemi, S.A. Parvez, C. Zheng, G. Hossain, Omicron variant of SARS-CoV-2: genomics, transmissibility, and responses to current COVID-19 vaccines, J. Med. Virol. 94 (2022) 1825–1832. https://doi:10.1002/jmv.27588.

[14] R. Yapasert, P. Khaw-on, R. Banjerdpongchai, Coronavirus infection-associated cell death signaling and potential therapeutic targets, Molecules 26 (2021) 7459, https://doi.org/10.3390/molecules26247459.

[15] M. Mohseni, H. Bahrami, B. Farajmand, F.S. Hosseini, M. Amanlou, H. Salehabadi, Indole alkaloids as potential candidates against COVID-19: an in silico study, J. Mol. Model. 28 (2022) 144, https://doi.org/10.1007/s00894-022-05137-4.
[16] V. Raj, J.-H. Lee, J.-J. Shim, J. Lee, Antiviral activities of 4H-chromen-4-one scaffold-containing flavonoids against SARS–CoV–2 using computational and *in vitro* approaches, J. Mol. Liquids 353 (2022), 118775, https://doi.org/10.1016/j.molliq.2022.118775.
[17] https://www.drugs.com/history/paxlovid.html. (Accessed 1 April 2023).
[18] https://www.drugs.com/history/paxlovid.html. (Accessed 1 April 2023).
[19] https://go.drugbank.com/unearth/q?utf8 %E2%9C%93&searcher=drugs&query=Paxlovid. (Accessed 1 April 2023).
[20] L. Agost-Beltrán, S. de la Hoz-Rodríguez, L. Bou-Iserte, S. Rodríguez, A. Fernández-de-la-Pradilla, F.V. González, Advances in the development of SARS-CoV-2 Mpro inhibitors, Molecules 27 (2022) 2523, https://doi.org/10.3390/molecules27082523.
[21] J. Chauhan, E. Cecon, N. Labani, F. Gbahou, F. Real, M. Bomsel, K.D. Dubey, R. Das, J. Dam, R. Jockers, S. Sen, Development of indolealkylamine derivatives as potential multi-target agents for COVID-19 treatment, Eur. J. Med. Chem. 249 (2023), 115152, https://doi.org/10.1016/j.ejmech.2023.115152.
[22] S.-i. Hattori, N. Higashi-Kuwata, H. Hayashi, S.R. Allu, J. Raghavaiah, H. Bulut, D. Das, B.J. Anson, E.K. Lendy, Y. Takamatsu, N. Takamune, N. Kishimoto, K. Murayama, K. Hasegawa, M. Li, D.A. Davis, E.N. Kodama, R. Yarchoan, A. Wlodawer, S. Misumi, A.D. Mesecar, A.K. Ghosh, H. Mitsuya, A small molecule compound with an indole moiety inhibits the main protease of SARS-CoV-2 and blocks virus replication, Nat. Com. 12 (2021) 668, https://doi.org/10.1038/ s41467-021-20900-6.
[23] R. Banerjee, L. Perera, L.M.V. Tillekeratne, Potential SARS-CoV-2 main protease inhibitors, Drug Discov. Today 26 (2021) 804–816, https://doi.org/10.1016/j.drudis.2020.12.005.
[24] M.A. Almaraz-Girón, E. Calderón-Jaimes, A.S. Carrillo, E. Díaz-Cervantes, E. C. Alonso, A. Islas-Jácome, A. Domínguez-Ortiz, S.L. Castañón-Alonso, Search for non-protein protease inhibitors constituted with an indole and acetylene core, Molecules 26 (2021) 3817, https://doi.org/10.3390/molecules26133817.
[25] M. Hassam, M.A. Bashir, S. Shafi, N.-u.-A. Zahra, K. Khan, K. Jalal, H. Siddiqui, R. Uddin, Identification of potent compounds against SARs-CoV-2: an in-silico based drug searching against Mpro, Comput. Biol. Med. 151 (2022), 106284, https://doi.org/10.1016/j.compbiomed.2022.106284.
[26] R. Arya, S. Kumari, B. Pandey, H. Mistry, S.C. Bihani, A. Das, V. Prashar, G. D. Gupta, L. Panicker, M. Kumar, Structural insights into SARS-CoV-2 proteins, J. Mol. Biol. 433 (2021), 166725, https://doi.org/10.1016/j.jmb.2020.11.024.
[27] M. He, Y. Huang, Y. Wang, J. Liu, M. Han, Y. Xiao, N. Zhang, H. Gui, H. Qiu, L. Cao, W. Jia, S. Huang, Metabolomics-based investigation of SARS-CoV-2 vaccination (Sinovac) reveals an immune-dependent metabolite biomarker, Front. Immunol. 13 (2022), 954801. https://doi:10.3389/fimmu.2022.954801.
[28] S.K. Mishra, T. Tripathi, One year update on the COVID-19 pandemic: where are we now? Acta Trop. 214 (2021), 105778 https://doi.org/10.1016/j.actatropica.2020.105778.
[29] A.K. Ghosh, J. Raghavaiah, D. Shahabi, M. Yadav, B.J. Anson, E.K. Lendy, S.-i. Hattori, N. Higashi-Kuwata, H. Mitsuya, A.D. Mesecar, Indole chloropyridinyl ester-derived SARS-CoV-2 3CLpro Inhibitors: enzyme inhibition, antiviral efficacy, structure−activity relationship, and X-ray structural studies, J. Med. Chem. 64 (2021) 14702–14714, https://doi.org/10.1021/acs.jmedchem.1c01214.
[30] N. Trivedi, A. Verma, D. Kumar, Possible treatment and strategies for COVID-19: review and assessment, Eur. Rev. Med. Pharmacol. Sci. 24 (2020) 12593–12608, https://doi.org/10.26355/eurrev_202012_24057.
[31] H. Chen, F. Cheng, J. Li, iDrug: integration of drug repositioning and drug-target prediction via cross-network embedding, PLoS Comput. Biol. 16 (2020), e1008040, https://doi.org/10.1371/journal.pcbi.1008040.
[32] A. Aktas, B. Tuzun, A.H.T. Kafa, K. Sayin, H. Ataseven, How do arbidol and its analogs inhibit the SARS-CoV-2? Bratislava Med. J. 121 (2020) 705–711. https://doi:10.4149/BLL_2020_115.
[33] H. Tanaka, S. Miyagi, Y. Yoshida, J.S. Lamb, C.N. Chick, L.P. Luhata, M. Shibata, E. Tanaka, Y. Suzuki, T. Usuki, Synthesis and biological evaluation of umifenovir analogues as Anti-SARS-CoV-2 agents, ChemistrySelect 7 (2022), e202202097, https://doi.org/10.1002/slct.202202097.
[34] Z. Zhu, Z. Lu, T. Xu, C. Chen, G. Yang, T. Zha, J. Lu, Y. Xue, Arbidol monotherapy is superior to lopinavir/ritonavir in treating COVID-19, J. Infect. 81 (2020), https://doi.org/10.1016/j.jinf.2020.03.060 e21–e23.
[35] L. Deng, C. Li, Q. Zeng, X. Liu, X. Li, H. Zhang, Z. Hong, J. Xia, Arbidol combined with LPV/r versus LPV/r alone against corona virus disease 2019: a retrospective cohort study, J. Infect. 81 (2020), https://doi.org/10.1016/j.jinf.2020.03.002 e1–e5.
[36] Y. Li, Z. Xie, W. Lin, W. Cai, C. Wen, Y. Guan, X. Mo, J. Wang, Y. Wang, P. Peng, X. Chen, W. Hong, G. Xiao, J. Liu, L. Zhang, F. Hu, F. Li, F. Zhang, X. Deng, L. Li, Efficacy and safety of Lopinavir/Ritonavir or Arbidol in adult patients with mild/moderate COVID-19: an exploratory randomized controlled trial, Méd. 1 (2020) 105–113, https://doi.org/10.1016/j.medj.2020.04.001.
[37] P. Xu, J. Huang, Z. Fan, W. Huang, M. Qi, X. Lin, W. Song, L. Yi, Arbidol/IFN-α2b therapy for patients with corona virus disease 2019: a retrospective multicenter cohort study, Microb. Infect. 22 (2020) 200–205, https://doi.org/10.1016/j.micinf.2020.05.012.
[38] S. Wei, S. Xu, Y.-H. Pan, Efficacy of arbidol in COVID-19 patients: a retrospective study, World J. Clin. Cases 9 (2021) 7350–7357. https://doi:10.12998/wjcc.v9.i25.7350.
[39] B. Mao, V.T.K. Le-Trilling, K. Wang, D. Mennerich, J. Hu, Z. Zhao, J. Zheng, Y. Deng, B. Katschinski, S. Xu, G. Zhang, X. Cai, Y. Hu, J. Wang, M. Lu, A. Huang, N. Tang, M. Trilling, Y. Lin, Obatoclax inhibits SARS-CoV-2 entry by altered endosomal acidification and impaired cathepsin and furin activity in vitro, Emerg. Microb. Infect. 11 (2022) 483–497, https://doi.org/10.1080/22221751.2022.2026739.
[40] R.J. Reiter, R. Sharma, F. Simko, A. Dominguez-Rodriguez, J. Tesarik, R.L. Neel, A. T. Slominski, K. Kleszczynski, V.M. Martin-Gimenez, W. Manucha, D.P. Cardinali, Melatonin: highlighting its use as a potential treatment for SARS-CoV-2 infection, Cell. Mol. Life Sci. 79 (2022) 143, https://doi.org/10.1007/s00018-021-04102-3.
[41] R. Zhang, X. Wang, L. Ni, X. Di, B. Ma, S. Niu, C. Liu, R.J. Reiter, COVID-19: melatonin as a potential adjuvant treatment, Life Sci. 250 (2020), 117583, https://doi.org/10.1016/j.lfs.2020.117583.
[42] E. Cecon, D. Fernandois, N. Renault, C.F.F. Coelho, J. Wenzel, C. Bedart, C. Izabelle, S. Gallet, S. Le Poder, B. Klonjkowski, M. Schwaninger, V. Prevot, J. Dam, R. Jockers, Melatonin drugs inhibit SARS-CoV-2 entry into the brain and virus-induced damage of cerebral small vessels, Cell. Mol. Life Sci. 79 (2022) 361, https://doi.org/10.1007/s00018-022-04390-3.
[43] S. Mehrzadi, M.Y. Karimi, A. Fatemi, R.J. Reiter, A. Hosseinzadeh, SARS-CoV-2 and other coronaviruses negatively influence mitochondrial quality control: beneficial effects of melatonin, Pharmacol. Ther. 224 (2021), 107825, https://doi.org/10.1016/j.pharmthera.2021.107825.
[44] S.A. Mousavi, K. Heydari, H. Mehravaran, M. Saeedi, R. Alizadeh-Navaei, A. Hedayatizadeh-Omran, A. Shamshirian, Melatonin effects on sleep quality and outcomes ofCOVID-19 patients: an open-label, randomized, controlled trial, J. Med. Virol. 94 (2022) 263–271. https://doi:10.1002/jmv.27312.
[45] Z.T. Hasan, M.Q.Y.M.A. Al Atrakji, A.K. Mehuaiden, The effect of melatonin on thrombosis, sepsis and mortality rate in COVID-19 patients, Int. J. Infect. Dis. 114 (2022) 79–84, https://doi.org/10.1016/j.ijid.2021.10.012.
[46] F. Rommasi, M.J. Nasiri, M. Mirsaeidi, Immunomodulatory agents for COVID-19 treatment: possible mechanism of action and immunopathology features, Mol. Cell. Biochem. 477 (2022) 711–726, https://doi.org/10.1007/s11010-021-04325-9.
[47] R. Begum, A.N.M. Mamun-Or-Rashid, T.T. Lucy, K. Pramanik, B.K. Sil, N. Mukerjee, P. Tagde, M. Yagi, Y. Yonei, Potential therapeutic approach of melatonin against omicron and some other variants of SARS-CoV-2, Molecules 27 (2022) 6934, https://doi.org/10.3390/molecules27206934.
[48] N.G. Fawazy, S.S. Panda, A. Mostafa, B.M. Kariuki, M.S. Bekheit, Y. Moatasim, O. Kutkat, W. Fayad, M.A. El-Manawaty, A.A.F. Soliman, R.A. El-Shiekh, A. M. Srour, R.F. Barghash, A.S. Girgis, Development of spiro-3-indolin-2-one containing compounds of antiproliferative and ant-SARS-CoV-2 properties, Sci. Rep. 12 (2022), 13880, https://doi.org/10.1038/s41598-022-17883-9.
[49] A.S. Girgis, S.S. Panda, A.M. Srour, A. Abdelnaser, S. Nasr, Y. Moatasim, O. Kutkat, A. El Taweel, A. Kandeil, A. Mostafa, M.A. Ali, N.G. Fawzy, M.S. Bekheit, E. M. Shalaby, L. Gigli, W. Fayad, A.A.F. Soliman, 3-Alkenyl-2-oxindoles: synthesis, antiproliferative and antiviral properties against SARS-CoV-2, Bioorg. Chem. 114 (2021), 105131, https://doi.org/10.1016/j.bioorg.2021.105131.
[50] J. Modranka, J. Drogosz-Stachowicz, A. Pietrzak, A. Janecka, T. Janecki, Synthesis and structure-activity relationship study of novel 3-diethoxyphosphorylfuroquinoline-4,9-diones with potent antitumor efficacy, Eur. J. Med. Chem. 219 (2021), 113429, https://doi.org/10.1016/j.ejmech.2021.113429.
[51] A.A. Babushkina, A.V. Dogadina, D.M. Egorov, J.L. Piterskaia, A.A. Shtro, Y. V. Nikolaeva, A.V. Galochkina, A.A. Kornev, V.M. Boitsov, Efficient synthesis and evaluation of antiviral and antitumor activity of novel 3-phosphonylated thiazolo [3,2-*a*]oxopyrimidines, Med. Chem. Res. 30 (2021) 2203–2215, https://doi.org/10.1007/s00044-021-02801-x.
[52] M. Bessières, E. Plebanek, P. Chatterjee, P. Shrivastava-Ranjan, M. Flint, C. F. Spiropoulou, D. Warszycki, A.J. Bojarski, V. Roy, L.A. Agrofoglio, Design, synthesis and biological evaluation of 2-substituted-6-[(4-substituted-1-piperidyl) methyl]-1H-benzimidazoles as inhibitors of ebola virus infection, Eur. J. Med. Chem. 214 (2021), 113211, https://doi.org/10.1016/j.ejmech.2021.113211.
[53] https://www.drugs.com/mtm/etidronate.html. (Accessed 1 April 2023).
[54] https://www.drugs.com/mtm/pamidronate.html. (Accessed 1 April 2023).
[55] https://www.drugs.com/mtm/alendronate.html. (Accessed 1 April 2023).
[56] https://www.drugs.com/mtm/zoledronic-acid.html. (Accessed 1 April 2023).
[57] https://www.drugs.com/cdi/ibandronate-tablets.html. (Accessed 1 April 2023).
[58] https://www.drugs.com/mtm/amifostine.html. (Accessed 1 April 2023).
[59] https://www.cancer.gov/about-cancer/treatment/drugs/amifostine. (Accessed 1 April 2023).
[60] M.A. Youssef, S.S. Panda, D.R. Aboshouk, M.F. Said, A. El Taweel, M. GabAllah, W. Fayad, A.A.F. Soliman, A. Mostafa, N.G. Fawzy, A.S. Girgis, Novel curcumin mimics: design, synthesis, biological properties and computational studies of piperidone-piperazine conjugates, ChemistrySelect 7 (2022), e202201406, https://doi.org/10.1002/slct.202201406.
[61] A.M. Srour, S.S. Panda, A. Mostafa, W. Fayad, M.A. El-Manawaty, A.A.F. Soliman, Y. Moatasim, A. El Taweel, M.F. Abdelhameed, M.S. Bekheit, M.A. Ali, A.S. Girgis, Synthesis of aspirin-curcumin mimic conjugates of potential antitumor and anti-SARS-CoV-2 properties, Bioorg. Chem. 117 (2021), 105466, https://doi.org/10.1016/j.bioorg.2021.105466.
[62] N.G. Fawzy, S.S. Panda, W. Fayad, E.M. Shalaby, A.M. Srour, A.S. Girgis, Synthesis, human topoisomerase IIα inhibitory properties and molecular modeling studies of anti-proliferative curcumin mimics, RSC Adv. 9 (2019) 33761–33774. https://doi:10.1039/c9ra05661k.
[63] N.G. Fawzy, S.S. Panda, W. Fayad, M.A. El-Manawaty, A.M. Srour, A.S. Girgis, Novel curcumin inspired antineoplastic 1-sulfonyl-4-piperidones: design, synthesis and molecular modeling studies, Anti Cancer Agents Med. Chem. 19 (2019) 1069–1078. https://doi:10.2174/1871520619666190408131639.
[64] K.A. Wyman, A.S. Girgis, P.S. Surapaneni, J.M. Moore, N.M. Abo Shama, S. H. Mahmoud, A. Mostafa, R.F. Barghash, Z. Juan, R.D. Dobaria, A.J. Almalki, T.

.

S. Ibrahim, S.S. Panda, Synthesis of potential antiviral agents for SARS-CoV-2 using molecular hybridization approach, Molecules 27 (2022) 5923, https://doi.org/10.3390/molecules27185923.

[65] I.A. Seliem, A.S. Girgis, Y. Moatasim, A. Kandeil, A. Mostafa, M.A. Ali, M. S. Bekheit, S.S. Panda, New pyrazine conjugates: synthesis, computational studies, and antiviral properties against SARS-CoV-2, ChemMedChem 16 (2021) 3418–3427, https://doi.org/10.1002/cmdc.202100476.

[66] I.A. Seliem, S.S. Panda, A.S. Girgis, Y. Moatasim, A. Kandeil, A. Mostafa, M.A. Ali, E.S. Nossier, F. Rasslan, A.M. Srour, R. Sakhuja, T.S. Ibrahim, Z.K.M. Abdel-samii, A.M.M. Al-Mahmoudy, New quinoline-triazole conjugates: synthesis, and antiviral properties against SARS-CoV-2, Bioorg. Chem. 114 (2021), 105117, https://doi.org/10.1016/j.bioorg.2021.105117.

[67] K.B. Lokhande, S. Doiphode, R. Vyas, K.V. Swamy, Molecular docking and simulation studies on SARS-CoV-2 M^{pro} reveals Mitoxantrone, Leucovorin, Birinapant, and Dynasore as potent drugs against COVID-19, J. Biomol. Struct. Dyn. 39 (2021) 7294–7305, https://doi.org/10.1080/07391102.2020.1805019.

[68] 3CL Protease (SARS-CoV-2) Assay Kit, BPS Bioscience, Catalog #79955-1, 6042 Cornerstone Court West, Ste. B, San Diego CA 92121, San Diego CA 92121. www.bpsbioscience.com.

[69] https://pubmed.ncbi.nlm.nih.gov/31643708/. (Accessed 1 April 2023).

[70] G.L. Plosker, D.P. Figgitt, Tipranavir, Drugs 63 (2003) 1611–1618. https://doi:10.2165/00003495-200363150-00009.

[71] J.S. Orman, C.M. Perry, Tipranavir: a review of its use in the management of HIV infection, Drugs 68 (2008) 1435–1463. https://doi:10.2165/00003495-200868100-00006.

[72] A.S. Girgis, S.S. Panda, M.N. Aziz, P.J. Steel, C.D. Hall, A.R. Katritzky, Rational design, synthesis, and 2D-QSAR study of anti-oncological alkaloids against hepatoma and cervical carcinoma, RSC Adv. 5 (2015) 28554–28569. https://doi:10.1039/c4ra16663a.

[73] Z.M. Nofal, A.M. Srour, W.I. El-Eraky, D.O. Saleh, A.S. Girgis, Rational design, synthesis and QSAR study of vasorelaxant active 3-pyridinecarbonitriles incorporating 1*H*-benzimidazol-2-yl function, Eur. J. Med. Chem. 63 (2013) 14–21, https://doi.org/10.1016/j.ejmech.2013.01.042.

[74] https://www.rcsb.org/structure/7C8U. (Accessed 1 April 2023).

[75] S. Das, U. Das, P. Selvakumar, R.K. Sharma, J. Balzarini, E. De Clercq, J. Molnár, J. Serly, Z. Baráth, G. Schatte, B. Bandy, D.K.J. Gorecki, J.R. Dimmock, 3,5-Bis (benzylidene)-4-oxo-1-phosphonopiperidines and related diethyl esters: potent cytotoxins with multi-drug-resistance reverting properties, ChemMedChem 4 (2009) 1831–1840. https://doi:10.1002/cmdc.200900288.